

1 **Title:** IRF3 regulates neuroinflammatory responses and the expression of genes  
2 associated with Alzheimer's disease.

3 **Authors:**

4 Radhika Joshi<sup>1</sup>, Veronika Brezani<sup>1</sup>, Gabrielle M Mey<sup>2,3</sup>, Sergi Guixé-Muntet<sup>4</sup>, , Marti  
5 Ortega-Ribera<sup>1</sup>, Yuan Zhuang<sup>1</sup>, Adam Zivny<sup>1</sup>, Sebastian Werneburg<sup>2,3</sup>, Jordi Gracia-  
6 Sancho<sup>4,5</sup>, Gyongyi Szabo<sup>1</sup>

7 **Affiliations:**

8 1 Department of Medicine, Beth Israel Deaconess Medical Center and Harvard Medical  
9 School, USA

10 2 Department of Ophthalmology and Visual Sciences, Kellogg Eye Center Michigan  
11 Neuroscience Institute, University of Michigan, Ann Arbor, USA

12 3 Michigan Neuroscience Institute, University of Michigan, Ann Arbor, MI, USA

13 4 Liver Vascular Biology, IDIBAPS Biomedical Research Institute- CIBEREHD,  
14 Barcelona, Spain

15 5 Department of Visceral Surgery and Medicine, Inselspital, Bern University Hospital,  
16 University of Bern, Bern, Switzerland

17

18

19

20

21

22

23 **Summary:** 144 words

24 The pathological role of interferon signaling is emerging in neuroinflammatory disorders,  
25 yet, the specific role of Interferon Regulatory Factor 3 (IRF3) in neuroinflammation  
26 remains poorly understood. Here, we show that global IRF3 deficiency delays TLR4-  
27 mediated signaling in microglia and attenuates the hallmark features of LPS-induced  
28 inflammation such as cytokine release, microglial reactivity, astrocyte activation, myeloid  
29 cell infiltration, and inflammasome activation. Moreover, expression of a constitutively  
30 active IRF3 (S388D/S390D:IRF3-2D) in microglia induces a transcriptional program  
31 reminiscent of the Activated Response Microglia and the expression of genes associated  
32 with Alzheimer's Disease, notably *apolipoprotein-e*. Lastly, using bulk-RNAseq of IRF3-  
33 2D brain myeloid cells, we identified Z-DNA binding protein-1 as a target of IRF3 that is  
34 relevant across various neuroinflammatory disorders. Together, our results identify IRF3  
35 as an important regulator of LPS-mediated neuroinflammatory responses and highlight  
36 IRF3 as a central regulator of disease-specific gene activation in different  
37 neuroinflammatory diseases.

38

39 **Keywords:**

40 IRF3, Type 1 interferon, ARM, IRM, Interferon response microglia, Neuroinflammation,  
41 Alzheimer's disease, DAM, Activated response microglia, ZBP1

42

## 43 **Introduction:**

44 Type I interferon (IFN-I) signaling is a critical adaptive immune response best known to  
45 combat viral infections <sup>1,2</sup>. The role of IFN-I signaling in the regulation of innate immunity  
46 and sterile inflammatory conditions is increasingly recognized. The pathological role of  
47 interferon signaling has been reported in a variety of neurological disorders including  
48 Alzheimer's disease (AD), Down syndrome, traumatic brain injury (TBI), and stroke <sup>3-8</sup>.  
49 Interferon signaling is also associated with behavioral changes such as cognitive decline,  
50 anxiety, depression, and susceptibility to stress <sup>9-11</sup>. Interferonopathies are another class  
51 of neuropathological disorders specifically classified as such based on their excessive  
52 activation of interferon signaling <sup>12</sup>. Relevant to the role of IFN-I, single nucleotide  
53 polymorphisms in interferon-stimulated genes (ISGs) have been associated with AD <sup>13</sup>.

54 Single-cell RNA sequencing techniques have discovered interferon-responsive  
55 microglia (IRMs with antiviral immune response) in diseases such as AD, multiple  
56 sclerosis and during natural aging <sup>14-16</sup>. IFN-responsive astrocytes and oligodendrocytes  
57 have also been described in AD models and aging <sup>17, 18</sup>. However, a comprehensive  
58 understanding of the underlying molecular mechanisms and function of these cell types  
59 is still under investigation.

60 Interferon signaling is regulated via 9 transcription factors called interferon response  
61 factors IRF1-9 <sup>19</sup>. Among these, IRF3 is at the crossroads of adaptive and innate immune  
62 responses. IRF3 activation is triggered downstream of TLR3, RIG-I, and MDA-5 in  
63 response to dsRNA, typically observed during viral infections <sup>19</sup>. IRF3 is also activated  
64 downstream of TLR4 in a MyD88 independent fashion involving the TRIF adapter  
65 molecule <sup>20, 21</sup>. Following TLR3/4 activation, IRF3 undergoes phosphorylation and  
66 dimerization leading to nuclear entry that drives the expression of ISGs <sup>19,21</sup>. While IRF3-  
67 mediated signaling has been well-studied in various models of peripheral inflammation <sup>20</sup>,  
68 <sup>22-25</sup>, in-depth studies directly investigating the role of IRF3 in neuroinflammatory  
69 conditions are lacking.

70 In this study, we examined the direct consequences of IRF3 perturbations on  
71 neuroinflammation and microglia. We used the commonly used model of

72 neuroinflammation induced by lipopolysaccharides (LPS), to mimic TLR4 activation. We  
73 observed that IRF3 plays a critical role in various features of LPS-mediated  
74 proinflammatory changes such as sickness behavior, cytokine production, myeloid cell  
75 infiltration and inflammasome activation. Furthermore, we showed that the mere  
76 expression of a constitutively active form of IRF3 (IRF3-2D) is sufficient to trigger a  
77 proinflammatory phenotype in microglia reminiscent of the IRMs. Importantly, IRF3  
78 activation leads to the expression of genes associated with AD, most notably,  
79 apolipoprotein-e (*apoe*). Lastly, we compared the transcriptome of brain myeloid cells  
80 from the IRF3-2D mouse model to that of other neuroinflammatory conditions. We  
81 identified *Zbp1* as one of the common proinflammatory signatures in microglia across  
82 different neurological disorders and we show that IRF3 directly regulates *Zbp1*. Taken  
83 together, we demonstrate that IRF3 plays an important role in proinflammatory responses  
84 induced by LPS. Furthermore, selective activation of IRF3 induces features of IRM and  
85 certain AD-associated genes.

## 86 **Results:**

### 87 **IRF3KO mice show attenuated sickness behavior and reduced proinflammatory** 88 **and IFN responses after an acute LPS challenge.**

89 To determine the relative contribution of the IRF3-induced signaling cascade on the  
90 proinflammatory effects of LPS, we first administered LPS (1mg/kg) to wild type (WT) and  
91 IRF3KO (whole body knockout) mice and euthanized mice 6 hours later. We analyzed  
92 LPS-induced sickness behavior (Fig 1A) in the open field test and observed that WT mice  
93 showed reduced locomotion and velocity ~5h after LPS administration compared to the  
94 vehicle group. This reduction in activity was significantly attenuated in the IRF3KO-LPS  
95 treated group (Fig 1B). Since sickness behavior is correlated to the peripheral and central  
96 nervous system (CNS) release of cytokines such as IL1 $\beta$ , TNF $\alpha$ , IL6 (Salvador et al 2021,  
97 Dantzer et al 2009), we assessed the levels of different cytokines and chemokines in  
98 cortical lysates to assess the state of neuroinflammation. We found a significant  
99 upregulation in IL1 $\beta$ , IL6, IL1 $\alpha$ , MCP1, and CXCL1 levels in the cortices of mice treated  
100 with LPS in the WT group (Fig 1C). However, cytokine (IL1 $\beta$ , IL1 $\alpha$ , IL6) and chemokine

101 (MCP1, CXCL1) induction by LPS was absent or significantly attenuated in IRF3KO mice  
102 (Fig 1C).

103 Since microglia are the key mediators of proinflammatory responses, we tested the  
104 expression of proinflammatory transcripts in flow-sorted microglia  
105 (CD11b<sup>+</sup>,CD45<sup>intermediate</sup>)(Fig 2A). IRF3 is critical for interferon responses downstream of  
106 TLR4, thus we first assessed signatures of interferon signaling followed by other  
107 proinflammatory mediators. LPS stimulation induced signatures of interferon signaling  
108 (*Ifit1*, *Isg15*, *Gbp2*) in WT mice, but ISG expression after LPS treatment was abrogated  
109 in IRF3KO mice (Fig 2B-D). Similarly, proinflammatory transcripts of *Cox2* and *H2-D1*  
110 were significantly increased in microglia of the WT-LPS but not in the IRF3KO-LPS group  
111 (Fig 2E,F). Interestingly, IRF3KO mice showed more sensitivity to LPS-induced C3  
112 transcripts compared to the WT (Fig 2G) and downregulation of the homeostatic marker  
113 *P2ry12* was comparable between WT and IRF3KO after acute LPS injection (Fig H).  
114 These data collectively suggested that IRF3 partially contributes to the proinflammatory  
115 effects of LPS in microglia.

116 IRF3 is expressed by all the major cell types in the brain including astrocytes<sup>26</sup>. Thus, we  
117 also tested the proinflammatory state of flow-sorted CD11b<sup>-</sup>ACSA-2<sup>+</sup> astrocytes in  
118 IRF3KO mice (Fig 2A). We observed that LPS-induced upregulation of interferon  
119 signaling (*Ifit*, *Gbp2*, and *Igtp* mRNA) (Fig2 I-K) and *Gfap* (Fig 2L) were significantly lower  
120 in the IRF3KO-LPS mice compared to the WT-LPS group, suggesting that IRF3 is  
121 important for LPS-mediated astrocyte activation (Fig 2I-L).

### 122 **IRF3KO mice show reduced myeloid cell infiltration and inflammasome activation** 123 **in the brain after repeated LPS challenges.**

124 IFN-I signaling is implicated in myeloid cell infiltration<sup>27</sup>. However, the contribution of IRF3  
125 specifically in the context of myeloid cell infiltration in the CNS is unexplored.

126 No monocyte infiltration was detected in response to 6h of single LPS injection in vivo in  
127 our model (Supplementary Fig 1A). Also, in chronic neuroinflammatory conditions TLR  
128 activation occurs constitutively or repeatedly. Thus, we next tested IRF3 activation and

129 its downstream effects in a repeated LPS challenge paradigm. Here, mice were treated  
130 with a 1mg/kg dose of LPS daily for 4 days and euthanized 6h after the last LPS dose  
131 (Fig 3A).

132 In the WT-LPS group, we observed a distinct population of CD11b<sup>+</sup>,CD45<sup>high</sup> cells, in  
133 addition to the resident microglia population defined as CD11b<sup>+</sup>,CD45<sup>intermediate</sup>,  
134 suggesting infiltration of peripheral myeloid cells upon repeated LPS challenges (Fig  
135 3B,C). In contrast to WT, IRF3KO mice showed significantly reduced percentage of  
136 infiltrating myeloid cells (Fig 3B, C). We also determined that this myeloid cell infiltration  
137 took place in the absence of damage to the blood-brain barriers in our model of 4-day  
138 LPS challenge as indicated by no changes in the expression of blood brain barrier  
139 markers, Claudin-1 and Occludin (Supplementary Fig 2A-C).

140 Moreover, the microglia population of IRF3KO-LPS group showed significantly lower  
141 CD11b expression (gated on the CD11b<sup>+</sup>,CD45<sup>intermediate</sup> microglia population) compared  
142 to the WT-LPS group (Fig 3D,E), further suggesting overall less proinflammatory effect of  
143 IRF3 deletion on microglia.

144 Because in the acute model we also observed proinflammatory transcripts in astrocytes,  
145 we tested whether astrocyte reactivity was also affected after 4 day repeated LPS  
146 challenge in IRF3 deficient mice. Assessment of GFAP levels in the cortex by western  
147 blots revealed a modest, yet significant, attenuation of GFAP levels in the IRF3KO-LPS  
148 mice compared to the WT-LPS mice (Fig 3F).

149 Because, we found attenuated IL1 $\beta$  induction in the cortex after acute LPS challenge in  
150 IRF3KO mice (Fig 1C) we were curious to see if IRF3 contributed to inflammasome  
151 priming and activation. The effect of IRF3 perturbations on IL1 $\beta$  induction and  
152 inflammasome activation have not been tested in the CNS. Surprisingly, we could not  
153 detect the hallmark features of inflammasome activation in the cortical samples of the  
154 acute LPS or 4-day LPS challenged WT mice (Supplementary Fig 1B,C). LPS-mediated  
155 inflammasome activation has also been reported before in the hippocampus<sup>28</sup>. Therefore  
156 we evaluated hippocampal lysates of the 4-day LPS challenged mice for inflammasome  
157 activation. Indeed we found, increased levels of pro- and cleaved- IL1 $\beta$  indicating

158 inflammasome priming and activation in the WT-LPS group compared to the WT-saline  
159 mice. This increase in pro- and cleaved- IL1 $\beta$  levels was significantly attenuated in the  
160 IRF3KO-LPS group compared to the WT-LPS group (Fig 3G). This data revealed a novel  
161 role of IRF3 in inflammasome activation in the CNS as well as in regional sensitivity to  
162 LPS-mediated inflammasome activation.

163 Together, this data complements the observations in our acute LPS model and suggests  
164 that IRF3 deletion provides protection against various proinflammatory features of  
165 repeated LPS challenges such as myeloid cell infiltration, astrocyte proliferation, and  
166 inflammasome activation.

167 **IRF3 deletion delays TLR4 signaling and dampens cytokine secretion in primary**  
168 **microglia cultures.**

169 To investigate the specific role of IRF3 in microglia, we assessed how IRF3 modulates  
170 LPS-induced TLR4 signaling cascade. TLR4 activation leads to MyD88 dependent and  
171 independent signaling cascade that can feedback onto each other <sup>21, 29, 30</sup>. To this end,  
172 we generated primary microglia cultures from WT and IRF3KO mice and challenged them  
173 in vitro with 20ng/ml LPS for various time points. We assessed phosphorylation of the key  
174 signaling cascades downstream of TLR4 activation: NF- $\kappa$ B (p65), p38, and ERK1/2 (Fig  
175 4A).

176 As expected, 30 min after in-vitro LPS addition, there was significant phosphorylation of  
177 the secondary signaling molecules- NF- $\kappa$ B (p65), p38, and ERK1/2 in the WT and  
178 IRF3KO microglia, as shown by the mean fold change >1 (over vehicle-treated samples)  
179 for phospho/total protein (Fig 4A, B). However, microglia isolated from IRF3KO mice  
180 showed strikingly lower phosphorylation levels of all the three signaling molecules at 30  
181 minutes. Notably, the phosphorylation of NF- $\kappa$ B continued to be significantly lower in the  
182 IRF3KO cultures for up to 120 min after LPS stimulation whereas p-p38 and pERK1/2  
183 were comparable to WT microglia (Fig 4A, C).



184 In addition, we observed significantly attenuated induction of cytokines in the supernatant  
185 of LPS-treated cultures of IRF3KO microglia (IFN $\beta$ , TNF $\alpha$ , IL6, and IL1 $\alpha$ ) when compared  
186 to the WT microglia (Fig 4D).

187 Together, our in vitro data shows an important regulatory role of IRF3 in LPS-mediated  
188 TLR4 signaling and cytokine production in microglia.

189 **Expression of a constitutively active form of IRF3 is sufficient to induce**  
190 **neuroinflammation.**

191 Phosphorylation of two serine residues (S388/390) is critical for IRF3 activation and  
192 nuclear translocation<sup>19</sup>. Previously a constitutively active form of IRF3 i.e. IRF3-2D  
193 (S388D/S390D) was shown to induce proinflammatory cascade in macrophages and  
194 adipocytes<sup>23</sup>. Thus, to specifically determine the effects of IRF3 activation in microglia,  
195 we expressed IRF3-2D in microglia using Cx3cr1Cre<sup>ERT2</sup> and IRF3-2D-Lox mice.

196 We confirmed the expression of IRF3-2D constructs in EFYP+ cells from the brain at the  
197 transcript and protein levels (Supplementary Fig 3A). We observed the characteristic  
198 protein doublet for IRF3-2D in EYFP+ cells<sup>23</sup>.

199 Similar to previous reports with Cx3cr1Cre<sup>ERT2</sup> mice, we observed leaky expression of  
200 IRF3-2D in the absence of tamoxifen and a strong trend in further increase with tamoxifen  
201 administration (supplementary Fig 3A, B)<sup>31</sup>. Therefore, we have also included additional  
202 Cre\_only controls (Cre\_Tam /Oil). Cre\_Tam and Cre\_Oil groups were very similar and  
203 thus data is pooled as a single group referred to as Cre\_only.

204 Tmem119+ microglia from tamoxifen-administered IRF3-2D\_Cre group (hereafter  
205 referred as IRF3-2D,Cre\_Tam) (Fig 5A-D) showed significant morphological changes  
206 with reduced branching and intersections, compared to the IRF3-2D,Cre\_Oil or Cre\_only  
207 group suggestive of a reactive microglia morphology (Fig 5A,C,D). The morphological  
208 changes in the branching did not lead to the changes in cell volume (Fig 5B).

209 Moreover, flow cytometry of IRF3-2D,Cre\_Tam brain samples revealed a distinct EYFP+  
210 CD11b+CD45<sup>high</sup> population of infiltrating monocytes in addition to Cd11b+CD45<sup>intermediate</sup>



211 microglia population (Fig 5E,F). This data corroborates the critical role of IRF3 in LPS-  
212 induced myeloid cell infiltration in the brain discussed earlier (Fig 3B,C). Moreover, the  
213 expression levels of CD45 and CD11b were elevated in the microglia population (gated  
214 on the Cd11b<sup>+</sup>CD45<sup>intermediate</sup>) of IRF3-2D,Cre\_Tam mice compared to that of Cre\_only  
215 mice (Fig 5G,H) further validating the proinflammatory microglia phenotype of IRF3-  
216 2D,Cre\_Tam group.

217 Additionally, IRF3-2D,Cre\_Tam mice also showed astrocyte reactivity in the cortex,  
218 suggesting that IRF3 activation is sufficient to mediate astrocyte reactivity (Fig 5I,J).

219 Taken together, these results demonstrate a proinflammatory role of IRF3 in microglia  
220 and astrocytes.

221 Despite this evidence of neuroinflammation, we found no significant behavioral changes  
222 in either of the anxiety tests (i.e. open field test and elevated plus maze) nor the Y-maze  
223 test, (Supplementary Fig. 4A-C) in the IRF3-2D,Cre\_Tam mice compared to  
224 IRF3-2D,Cre\_Oil or Cre\_only group.

225 To gain deeper insights into the proinflammatory profile of IRF3-2D expressing cells, we  
226 performed bulk-RNA sequencing on flow sorted Cx3cr1<sup>+</sup>(EYFP<sup>+</sup>) population of myeloid  
227 cells from the brain (cortex, subcortical areas, and hippocampus).

228 To account for changes induced by tamoxifen administration, we compared the  
229 transcriptome of IRF3-2D,Cre\_Tam EYFP<sup>+</sup> population with that of Cre\_Tam. We  
230 observed in total 908 genes that were differentially regulated in response to the presence  
231 of IRF3-2D. The expression of IRF3-2D in microglia resulted in a proinflammatory  
232 transcriptome enriched with the pathways related to IFN- $\beta$ , IFN- $\gamma$ , and viral responses  
233 (Fig 6A, B). In addition, we observed upregulation of pathways related to leukocyte  
234 migration, and cell adhesion further strengthening the effect of IRF3 on myeloid cell  
235 infiltration observed in this study (Fig 3B,C & 5E,F). We also found upregulation of  
236 pathways related to antigen presentation and co-stimulatory molecules [*H2 (-Ab1,- Eb1,*  
237 *-Aa, -Q6, -Q7, -K1, -D1, -Q5, -M3, -Dma,- K2, -T22, -Q4), Tap1, Cd74, Cd40, Cd72,*

238 immunoproteasome (*Psmb9*, *Psme1*, *Psme 2*), cytoskeletal reorganization and ER-  
239 phagosome, providing further insights into the proinflammatory role of IRF3.

240 The top differentially regulated genes in this comparison were the subset of genes  
241 associated with AD. These included genes such as *ApoE*, *Axl*, *Cd74*, *Fth1*, *Itgax*, and  
242 *Ctsb* (Fig 6B). As *ApoE*, was the top candidate, we validated its expression at the protein  
243 level. We observed that APOE expression was significantly upregulated in Tmem119+  
244 microglia in IRF3-2D,Cre\_Tam group compared to IRF3-2D,Cre\_Oil or Cre\_only group  
245 (Fig 6C,D).

246 Microglia from the AD and neurodegenerative models show particular gene signatures  
247 which are termed as activated response microglia (ARM), or disease associated microglia  
248 (DAM) or microglia neurodegenerative phenotype (MGnD) with overlapping features <sup>14</sup>,  
249 <sup>32-34</sup>. In addition, interferon responsive microglia i.e. IRMs have also been reported in AD  
250 and aged mouse brains <sup>14</sup>, <sup>16</sup>. Therefore, we wondered what proportion of EYFP+ cells  
251 from IRF3-2D animals showed gene signatures associated with IRMs and AD. We  
252 performed data deconvolution with single cell RNA seq data to determine the cell fractions  
253 in IRM and ARM-like cells <sup>14</sup>. The presence of IRMs was observed in IRF3-2D,Cre\_Tam  
254 mice (Fig 6E) in line with the increased interferon signaling observed (Fig 6A).  
255 Interestingly, we observed significantly increased population of ARM in IRF3-  
256 2D,Cre\_Tam group compared to the Cre\_only group, and a strong trend in increase  
257 ( $p < 0.09$ ) compared to IRF3-2D\_Oil group (Fig 6E). IRF3-2D,Cre\_Oil group also showed  
258 presence of IRM and increasing trend in ARM population compared to the Cre\_only  
259 controls, reflecting on the leaky expression of IRF3-2D and associated proinflammatory  
260 signaling in this model (Fig 6E, Supplementary Fig 5). Nonetheless, these results show  
261 that IRF3-mediated signaling is sufficient to induce IRM and ARM signatures in microglia.  
262 Thus, we conclude that IRF3 plays a critical role in microglia-mediated proinflammatory  
263 responses and regulates expression of genes associated with AD.

264 **Expression of ZBP1, a target of IRF3, is upregulated in microglia in various**  
265 **neuroinflammatory conditions.**

266 To further dissect the molecular mechanism and genes regulated by IRF3 signaling in  
267 microglia beyond LPS challenge or IRF3-2D model, we compared the transcriptome of  
268 IRF3-2D overexpressing EYFP<sup>+</sup> cells to that of microglia from various neuroinflammatory  
269 conditions such as AD (5XFAD), Tauopathy model, LPS challenge, and glioma<sup>35</sup>. In each  
270 data set, we used differentially upregulated genes showing a Log fold change of >0.6 and  
271 adjusted p-value of <0.05. From these comparisons, we identified 10 genes, comprising  
272 direct and indirect targets of IRF3, that are of relevance across different  
273 neuroinflammatory conditions (Fig 7A). IRF3-mediated changes in the transcriptome  
274 primarily result from the direct transcriptional activity of IRF3 or IRF3-mediated secondary  
275 signaling cascades. The direct transcriptional targets of IRF3 have been previously  
276 identified by ‘Cleavage Under Targets and Release Using Nuclease’ (CUT and RUN)  
277 technique from hepatocytes expressing IRF3-2D<sup>22</sup>. Of these 10 common genes, 3 genes  
278 were identified as direct transcriptional targets of IRF3- *Oasl2*, *Zbp1* and *Tlr2* by CUT and  
279 RUN<sup>22</sup>.

280 In view of the novelty, we particularly focused on *Zbp1*. *Zbp1* was initially recognized as  
281 interferon-inducible tumor-associated protein<sup>36</sup>. ZBP-1 is shown to be critical for LPS-  
282 mediated production TNF $\alpha$  and IFN $\beta$  in macrophages<sup>37</sup>. However, the role of ZBP1 in  
283 neurological disorders remains poorly studied. Thus, we aimed to validate *Zbp1* as the  
284 target of IRF3 in our models of LPS challenge in the CNS.

285 We observed that after an in vivo acute LPS challenge *Zbp1* mRNA was significantly  
286 induced in microglia and astrocytes isolated from the WT-LPS group, while no change  
287 could be detected in cells isolated from the IRF3KO mice (Fig 7B,C). Similarly, there was  
288 a striking increase in the expression of *Zbp1* (~2.5 fold) in WT microglia cultures treated  
289 with LPS in-vitro when compared to IRF3KO primary microglia 6h after LPS stimulation  
290 (Fig 7D). This data corroborated results from the in vivo 4-day repeated LPS challenge  
291 model, where only the WT, and not the IRF3 deficient, brain tissue showed significantly  
292 elevated levels of *Zbp1* protein after LPS treatment (Fig 7E).

293 Thus, together we identify Zbp1 as a novel proinflammatory target common across  
294 different neuroinflammatory conditions and show that Zbp1 expression is regulated by  
295 IRF3-induced signaling in microglia and astrocytes.

## 296 **Discussion:**

297 In this manuscript, we demonstrate that the expression of IRF3 in microglia is important  
298 in different neuroinflammatory contexts and IRF3 activation and IRF3-mediated signaling  
299 is sufficient to drive expression of AD-related genes. We also discovered that LPS-  
300 induced astrocyte activation is also dependent on IRF3. The function of IRF3 has been  
301 extensively studied in peripheral models of TLR3 and TLR4 activation i.e. viral and  
302 bacterial infection, respectively, including our work on IRF3 in sterile inflammatory  
303 conditions such as alcohol abuse and obesity<sup>23, 24, 38</sup>. Role of IRF3 has been studied in  
304 viral encephalitis. Phosphorylation deficient mutation at S386 of IRF3 is associated with  
305 reduced IFN-I signaling in Herpes simplex encephalitis (HSE) patients<sup>39</sup>. IRF3KO mice  
306 showed higher mortality rates and increase inflammation on HSE infection<sup>40</sup>. Similarly,  
307 IRF3 deficient mice showed inability to resolve inflammation in the CNS by alphavirus  
308 infection<sup>41</sup>. In this report we evaluated the cell type-specific contribution of IRF3 in  
309 microglia and its impact in a broader context of neuroinflammation.

310 Using LPS, a prototypical pathogen-associated molecular pattern (PAMP) and TLR4  
311 ligand, we observed that IRF3 is involved in the production and release of the key  
312 inflammation-associated cytokines and chemokines, sickness behavior as well as Type 1  
313 interferon-dependent genes in the brain. Other mediators, such as TNF $\alpha$  and IFN $\beta$  also  
314 contribute to sickness behavior, however, we could not detect a significant amount of  
315 these cytokines in the cortex of mice at 6h post LPS stimulation when other markers were  
316 assessed in our experiments<sup>42, 43</sup>.

317 Activation of TLR4, a widely studied pattern recognition receptor, has been observed in  
318 myriad of neuropathologies ranging from gram-negative bacterial infections (mimicked  
319 here by LPS), AD, Parkinson's disease (PD), multiple sclerosis to amyotrophic lateral  
320 sclerosis<sup>44-47</sup>. TLR4 also senses both pathogen-associated molecular patterns, such as  
321 LPS, and sterile inflammatory signals, for example HMGB1<sup>48, 49</sup>. Furthermore, LPS

322 primes brain responsiveness to HMGB1<sup>50</sup>. Thus detailed understanding of TLR4  
323 mediated downstream signaling in CNS is warranted. TLR4 triggers two downstream  
324 pathways through adaptor proteins: MyD88 and TRIF dependent leading to MyD88  
325 independent signaling<sup>51</sup>. While much attention is paid to MyD88-dependent or NF- $\kappa$ B-  
326 mediated signaling, here we highlight the role of IRF3 in TLR4/LPS-mediated  
327 inflammatory responses in neuroinflammation.

328 In addition to TLR4, IRF3 can also be activated intracellularly via the cGAS-STING  
329 pathway as well as via endoplasmic reticulum stress via STING<sup>38, 52, 53</sup>. Microbial or  
330 endogenous DNA is recognized through cGAS-STING pathway and culminates in IRF3  
331 activation<sup>52</sup>. cGAS-STING activation is observed in various neuroinflammatory conditions  
332 such as AD, TBI, PD, aging etc.<sup>6, 7, 54</sup>, indirectly implicating IRF3 in these conditions and  
333 emphasizing the need to study functions of IRF3 in the CNS.

334 In neuroinflammatory diseases there is continued presence of disease associated  
335 molecular patterns (DAMPs) and/or PAMPs that sustain inflammation. Thus, we also  
336 tested a four-day model of repeated LPS stimulations where we discovered a novel role  
337 of IRF3 in monocyte infiltration and inflammasome activation in the CNS. The IFN  
338 response in the CNS has been associated with myeloid cell infiltration under tumorigenic  
339 conditions and viral infections<sup>27, 55</sup>, however, the specific role of IRF3 in myeloid cell  
340 infiltration in the brain has not been described previously. The reduced myeloid cell  
341 infiltration observed in the IRF3KO-LPS group in the 4-day model correlates with the  
342 reduced levels of MCP1 seen in the acute model in Fig 1C. Interestingly, at 4 day time  
343 point, we could not detect MCP1 anymore in the samples, suggesting that MCP1 release  
344 in the initial LPS challenge is sufficient to elicit myeloid cell infiltration in the brain.

345 In our study, reduced NLRP3 inflammasome activation modulated by IRF3 deletion in the  
346 CNS was another novel finding. This observation is significant in light of the critical role  
347 of NLRP3 in AD, and other neurological disorders<sup>56, 57</sup>. This result is in line with the  
348 previous observations made by our lab and others showing reduced NLRP3  
349 inflammasome activation in the absence of IRF3 in the peripheral models of inflammation  
350<sup>24, 58</sup>.

351 IRF3 is expressed in the brain by microglia, astrocytes, neurons, endothelial cells and  
352 oligodendrocytes<sup>26</sup>. As astrocytes have increasingly gained importance to partake in  
353 regulating immune responses in the brain, we assessed the responses from astrocytes.  
354 Indeed we found a significant reduction in the LPS-induced proinflammatory response of  
355 astrocytes in the absence of IRF3 expression in both the *in vivo* models of LPS that we  
356 tested, suggesting a major role for IRF3 in astrocyte responses to acute as well as  
357 repeated LPS challenges. Proinflammatory responses of microglia contribute to astrocyte  
358 activation, however, in our study we cannot distinguish between microglia dependent or  
359 astrocyte autonomous role of IRF3 in LPS-mediated astrocyte activation<sup>17, 59</sup>.

360 LPS-induced upregulation of proinflammatory transcripts in microglia of WT and IRF3KO  
361 mice, showed partial dependence on IRF3. Surprisingly, we observed complement factor  
362 C3 transcripts were upregulated in IRF3KO-LPS microglia compared to WT-LPS groups.  
363 This finding is surprising since C3 is a known target of IFN-I<sup>4, 60</sup> and is also significantly  
364 upregulated in IRF3-2D expressing myeloid cells (Fig 6B). A compensatory effect of LPS-  
365 mediated IRF3-independent pathway of complement activation may explain this effect<sup>61</sup>.  
366 Moreover, microglia transcripts from IRF3KO mice showed elevated levels of the  
367 homeostatic marker *P2ry12* compared to the WT. However, solely based on this result it  
368 is difficult to draw conclusions on the homeostatic state of microglia in these mice.  
369 Analysis of the transcriptome of IRF3KO mice microglia may shed light on this aspect.

370 To determine the role of IRF3 in LPS-mediated signaling in microglia we used primary  
371 microglia cultures derived from WT and IRF3KO pups. As seen in the cortical lysates,  
372 LPS-induced cytokine release in the supernatant was reduced in IRF3KO microglial  
373 cultures compared to WT. Furthermore, we observed that IRF3 deletion directly  
374 modulated the signaling events downstream of TLR4 particularly in the first 30 min  
375 compared to 120 min, suggesting that effects of IRF3 deletion are compensated by the  
376 feedback loops between secondary messengers downstream of TLR4 signaling.

377 IRF3KO mice have been shown to have reduced peripheral inflammation in response to  
378 LPS<sup>25</sup>. Our *in vitro* results showed reduced cytokine levels and proinflammatory  
379 responses of isolated IRF3 deficient microglia compared to wild type, indicating that the



380 observed reduction in neuroinflammation in vivo in IRF3 KO mice was not just an outcome  
381 of reduced peripheral inflammation but also reduced intrinsic inflammatory response of  
382 IRF3KO microglia to LPS challenge.

383 While our data in IRF3KO mice and cells indicated the importance of this pathway in  
384 TLR4-mediated neuroinflammation, next, to understand the isolated effects of IRF3  
385 activation in microglia we took advantage of the IRF3-2D-lox line, described previously  
386 <sup>23</sup>. Our data indicate that constitutive IRF3 activation in microglia results in key features  
387 of neuroinflammation including increased monocyte infiltration to the brain and increased  
388 GFAP expression suggesting astrocyte activation. We also found that a key feature of  
389 IRF3-2D expression was the upregulation of certain DAM genes, or ARMs, most notably  
390 *ApoE*. *ApoE* is a major risk factor for the late onset Alzheimer's disease. In addition, *ApoE*  
391 expression in microglia has been shown to regulate microglia immunometabolism  
392 influencing their ability to respond to A $\beta$  plaques, and tauopathy <sup>32, 62-64</sup>. APOE-TREM2  
393 pathway has been shown to be important for expression of DAM and ARM genes <sup>14, 32</sup>.  
394 Our model of IRF3-2D, suggests that sustained IRF3 activation is sufficient to drive the  
395 expression of *ApoE*, which in turn can regulate the expression of certain genes associated  
396 with microglia phenotype in neurodegenerative diseases. *ApoE* is not one of the known  
397 transcriptional targets of IRF3; our study suggests that it may be upregulated through  
398 IRF3-mediated mechanisms. Further investigation is needed to determine the exact  
399 mechanism of IRF3-mediated upregulation of APOE.

400 Since the bulk RNAseq performed from IRF3-2D,Cre\_Tam mice comprises EYFP<sup>+</sup> cells  
401 in the brain i.e. microglia and infiltrating myeloid cells, we ascertained microglia specific  
402 effects by visualizing Tmem119<sup>+</sup> cells for morphological analysis (Fig 5A), and APOE  
403 expression (Fig 6C) and using CD11b<sup>+</sup>CD45<sup>intermediate</sup> gate for assessing levels of CD11b  
404 in Fig 5G,H). We also compared the transcriptome of EYFP<sup>+</sup> cells devoid of infiltrating  
405 myeloid cells from IRF3-2D,Cre\_Oil with Cre\_Oil groups (Fig 5E,F and Supplementary  
406 Fig 5). This comparison showed a total of 321 differentially regulated genes (DEGs),  
407 fewer than the 908 DEGs described in IRF3-2D,Cre\_Tam group in Fig 6. Here, we  
408 observed proinflammatory pathways and genes such as *Axl*, *Cybb*, *Cst7*, *H2-D1*, *Cd74*  
409 (Supplementary Fig 5) and increasing trend in ARM fraction (Fig 6E), collectively showing



410 proinflammatory effect of IRF3-2D activation on microglia in the absence of infiltrating  
411 myeloid cells.

412 While these results clearly establish effects of IRF3-2D on microglia, we cannot rule out  
413 the effect of leaky expression of IRF3-2D in Cx3CR1<sup>+</sup> myeloid cells in the periphery and  
414 further experiments would be needed to tease those apart. It is interesting to note that  
415 Tamoxifen administration further increased the ARM-like fraction in IRF3-2C,Cre\_Tam  
416 group while the IRM-like fraction shows no additive effect, it is possible that the expression  
417 of ARM related genes is induced by targets of IRF3 not directly involved in IFN-I signaling  
418 (CUT and RUN analysis <sup>22</sup>). Previously, IFN-I signaling in microglia has been associated  
419 with increased anxiety <sup>9, 65</sup>, however despite induction of such a strong IFN-I signaling  
420 cascade in the IRF3-2D brains, we found no obvious behavioral changes in anxiety or  
421 memory performance of these mice. In our model we cannot rule out the development of  
422 any compensatory behavioral and transcriptional changes that may mask the subtle  
423 underlying behavioral abnormalities. Moreover, in this model we see IRF3-mediated  
424 signaling which may not recapitulate the full spectrum of inflammation and IFN-I signaling  
425 observed by others (Ben-Yehuda et al., 2020, Sahasrabudde and Ghosh, 2022).

426 Lastly, to evaluate the presence of signatures of IRF3 activation and IFN-I signaling in  
427 different proinflammatory disorders, we compared the genes upregulated with IRF3-2D  
428 expression to that of the genes upregulated in different neuroinflammatory disorders such  
429 as glioma, Alzheimer's disease model of amyloid and tauopathy, and LPS challenge. Of  
430 these 10 common genes, we were particularly interested in Zbp1. Zbp1 is known for its  
431 function in cell death pathways, viral response and inflammasome activation <sup>36</sup>. In  
432 addition, the role of Zbp1 in proinflammatory signaling, independent of cell death, is also  
433 emerging <sup>66</sup>. However, there are limited studies investigating the role of Zbp1 in  
434 neuroinflammation and its role in AD is beginning to emerge <sup>67</sup>.

435 Previous studies have shown Zbp1 to be a regulator of IRF3 <sup>37</sup>. We recently showed that  
436 Zbp1 expression is modulated by IRF3 in mouse models of cholestatic-liver injury <sup>24</sup>. Here  
437 we show for the first time that IRF3 can directly regulate Zbp1 levels in microglia and  
438 astrocytes.

439 Taken together we discovered new insights into the role of IRF3 in promoting  
440 neuroinflammation specifically, in microglia and highlight IRF3 and its downstream genes  
441 as important players in various neuroinflammatory conditions.

442

443

444 **STAR Methods:**

445 Mice: The following mice were used- C57BL/6 from Jax mice (000664), IRF3KO  
446 (described previously,<sup>24</sup>, Cx3cr1<sup>CreERT2</sup>(B6.129P2(Cg)-  
447 Cx3cr1tm2.1(cre/ERT2)Litt/WganJ-021160), IRF3-2D (C57BL/6-  
448 Gt(ROSA)26Sortm4(CAG-Irf3\*S388D\*S390D)Evdr/J-036261). All strains were in  
449 C57BL/6J background. The mice were maintained on ad-libitum food and water. All the  
450 breedings, experiments and euthanasia were conducted as per the institutional IACUC  
451 protocol 030-2022. Both the sexes between the ages of 3-6 months were used.

452 Tamoxifen preparation: Tamoxifen stocks of 20mg/ml were prepared by dissolving  
453 Tamoxifen in Corn oil at 37°C. Mice were given oral gavage 10mg/kg of Tamoxifen or  
454 equal volume oil for consecutive 5 days and used for experiment 5 weeks later.

455 LPS preparation and administration: LPS was prepared by dissolving LPS in saline at  
456 1mg/mL and intraperitoneally injected in mice at 1mg/kg dose as indicated. For in vitro  
457 experiments LPS was dissolved in water at 100ug/mL concentration and diluted in media  
458 just before addition.

459 Microglia and astrocyte flow cytometry: Microglia and astrocytes were flow sorted as  
460 described previously<sup>68</sup>. Briefly, mice were transcardially perfused and brains were  
461 dissected out. One half of the brains were fixed in 4%PFA overnight. From the other half  
462 the prefrontal cortex, hippocampus and cerebellum were dissected out and frozen on dry  
463 ice. The rest of the brain was homogenized in ice-cold HBSS (Ca<sup>++</sup>, Mg<sup>++</sup> free). Cells were  
464 pelleted at 350g for 7 min followed by a 37% percoll plus spin without brakes. The top  
465 layer of myelin was aspirated and the microglia pellet was washed in HBSS before  
466 staining. The cell pellet was incubated in FC block (1:50) at 4°C for 5 min followed by  
467 incubation in antibodies against CD11b, CD45, and ACSA-2 in FACS buffer (2% Fetal  
468 Bovine Serum in PBS Ca<sup>++</sup>, Mg<sup>++</sup> free) at 4°C for 20 min. DAPI (1mg/ml, 1:1000) was  
469 added in the last 5 min of antibody incubation. The cells were washed in FACS buffer and  
470 sorted using Cytoflex-SRT or analyzed on Cytex Aurora. Microglia were sorted as  
471 Cd11b<sup>+</sup>, CD45<sup>intermediate</sup> population and astrocytes were sorted as CD11b<sup>-</sup>, ACSA-2. For  
472 mice in Cx3cr1<sup>CreERT2</sup> background cells were sorted using EYFP fluorescence. Sorted

473 cells were pelleted and stored at  $-80^{\circ}\text{C}$  until downstream processing. 15-20K microglia  
474 were used for western blotting. Flow data was analyzed using FlowJo.

475 Primary microglia cultures: Primary microglia were cultured as described previously with  
476 slight modification<sup>69</sup>. Brains from the WT and IRF3KO pups (0-4 days old) were  
477 dissected, meninges removed, and homogenized with mortar and pestle. Cells were  
478 pelleted by centrifugation at 350g for 7min at  $4^{\circ}\text{C}$  and directly plated onto Poly-D-Lysine  
479 (PDL) coated (10ug/mL) 90mm dishes. Cells were cultured in DMEMF-12 containing 10%  
480 FBS and 1% Penicillin/Streptomycin. Cultures were grown at a standard 5%  $\text{CO}_2$ ,  $37^{\circ}\text{C}$   
481 incubator. Next day cultures were washed 3 times with phosphate-buffered saline and  
482 incubated for an additional 3-4 days in the culture medium described above before the  
483 addition of the growth factors (mCSF and  $\text{TGF}\beta$ ). 2-3 days later microglia were shaken  
484 off the astrocyte monolayer and harvested every 3rd day for 3 cycles. Harvested microglia  
485 were plated on PDL coated 12 well dish at  $4 \times 10^5$  cells per/mL in plain DMEM-F/12  
486 without FBS a day before the experiment. On the day of the experiment, cells were treated  
487 with LPS (20ng/mL) for an indicated amount of time, and supernatant and cells were  
488 harvested for further analysis. The supernatant was spun at 10K for 10 min at  $4^{\circ}\text{C}$  and  
489 stored at  $-80^{\circ}\text{C}$  until further use. Cells in each well were washed in ice-cold PBS before  
490 harvesting.

491 Western Blotting: RIPA was used as a lysis buffer with a Protease and Phosphatase  
492 inhibitor cocktail. Brain tissue was lysed in the tissue homogenizer, followed by a spin at  
493 10K for 10 min at  $4^{\circ}\text{C}$ . A predetermined number of cells as indicated above was loaded  
494 for western blots from primary microglia cultures or flow-sorted microglia. Total of 50ug  
495 of protein was loaded onto SDS gels from tissues. Proteins were transferred onto  
496 nitrocellulose membranes and blocked in 5% BSA in 0.1% TBST at room temperature  
497 (RT) for 1h. Blocked membranes were incubated with primary antibodies in 5% BSA  
498 overnight and washed 3 times in 0.1% TBST. A secondary antibody was added in  
499 blocking solution for 1h at RT followed by 3 washes in 0.1% TBST before developing the  
500 blot.

501 For western blots from primary microglia in Figure 4B & C, the results are represented as  
502 a comparison between WT and IRF3KO cultures. For signaling cascades the  
503 phosphorylation levels are represented as = (LPS-treated [Phospho protein/ Total  
504 protein]) / (Saline-treated [Phospho protein/ Total protein]) for WT and IRF3KO cultures  
505 separately.

506 Immunohistochemistry and image analysis: Brains were fixed in 4% PFA overnight,  
507 followed by cryopreservation in 30% sucrose solution until the brains sank. Brains were  
508 sectioned using Leica cryostat into 25 $\mu$ m thin sections, collected in 0.05% Sodium Azide  
509 solution in PBS, and stored at 4 $^{\circ}$ C until stained. Desired brains were mounted onto glass  
510 slides, washed in PBS and blocked using 1% Triton and 10% Horse Serum in PBS for 1h  
511 at RT. Primary antibodies were dissolved in the blocking and incubated overnight at 4 $^{\circ}$ C.  
512 Primary antibodies were washed at RT in 1% Triton in PBS and incubated in secondary  
513 antibodies in 1% Triton and 1% Horse serum for 1h at RT. After secondary antibody  
514 incubation, DAPI (1mg/ml at 1:1000) solution was added for 5 min at RT followed by 2  
515 washes with 1% Triton in PBS. Sections were imaged at 63x magnification on a Zeiss  
516 LSM-700 confocal microscope. Iba $^{+}$  staining was used for morphometry analysis. In Fig  
517 5A, the sections were co-stained with Tmem119, a microglia specific marker, to verify the  
518 microglial identity of the cells. The filament tracer module and Sholl analysis extension in  
519 Imaris (Bitplane; Zurich, Switzerland) were used to assess microglia morphometry.

520 Bulk-RNA seq: 1000 sorted microglia were suspended in 1% beta-mercaptoethanol in  
521 TCL buffer and sequenced using smart-seq2 platform at Broad Institute. Briefly, the raw  
522 sequencing reads were quality-checked and data were pre-processed with Cutadapt  
523 (v2.5) for adapter removal. Gene expression quantification was performed by aligning  
524 against the GRCm38 genome using STAR (v2.7.3a). Reads were quantified against  
525 Ensembl v98 annotated transcript loci with feature Counts (Subread 1.6.2). Differential  
526 gene expression analysis was performed using DESeq2 (v1.24.0) while ClusterProfiler  
527 (v3.12.0) was utilized for downstream functional investigations. Plots were generated in  
528 R using ggplot2 (v3.3.3), EnhancedVolcano (v1.8.0) , ComplexHeatmap (v2.6.2).

529 For deconvolution analyses we reanalyzed previously published single-cell expression  
530 data as described in the original manuscript (GSE127884). The data containing labels for  
531 ARM and IRM cell types was uploaded to the CIBERSORTx platform in order to generate  
532 a signature matrix for these cell populations. This matrix was used in combination with  
533 our bulk RNA data in order to estimate the relative amounts of each of the cell types.

534 RNA isolation and qRT PCR: RNA was isolated from microglia and astrocyte pellets using  
535 Qiagen RNeasy plus micro kit. cDNA was converted using the Superscript II kit. Gene  
536 expression analysis was conducted by qRT PCR using SYBR green from BioRad. Gene  
537 expression for every sample was normalized to 18s rRNA as housekeeping gene.

538 Elisa: Cytokine levels were detected using Elisa kits. Plates were coated as per  
539 manufacturer's instructions. Cell culture supernatant or tissue lysates (prepared as  
540 described above) were incubated overnight at 4<sup>0</sup>C. Kit-specific protocol was followed for  
541 washing and developing of the Elisa plate. Absorbance was measured on a microplate  
542 reader and the amount of the cytokine was estimated based on the standard curve.

543 Animal behavior: Mice were brought into the behavior room 30 min before the experiment.  
544 Animal behavior was recorded for 5 min for all tests with an overhead camera and  
545 analyzed using Ethovision<sup>XT</sup>. 20 lux light intensity was maintained in the room. Animal  
546 behavior was conducted between 9am-2pm. The position of the animal was monitored  
547 using the center of mass body point. The behavior tests were performed at least 24h  
548 apart.

549 For an open field test, 40cm x 40cm x 40cm arena was used. Mice were released in the  
550 center of the arena, facing away from the experimenter. As indicated in the figures, the  
551 total distance traveled, velocity and time spent in the center were calculated to determine  
552 anxiety-like behavior or sickness behavior. The central zone was marked 5 cm away from  
553 the walls of the arena.

554 For the elevated plus maze, mice were released into the central zone facing the open  
555 arms away from the experimenter. Total time spent in the open arms was used as the  
556 measure of anxiety. The length of each arm was 20 cm.

557 Y maze test was used to assess memory performance in mice. The Y maze test was  
558 performed last, where mice were allowed to explore the arena, and memory was  
559 assessed based on the pattern of spontaneous arm alternation. The length of the arms  
560 was 15 cm each.

561 Statistics: Data was plotted as mean  $\pm$  SEM using GraphPad Prism 9. The appropriate  
562 statistical test is indicated in the figure legend for each comparison.

563

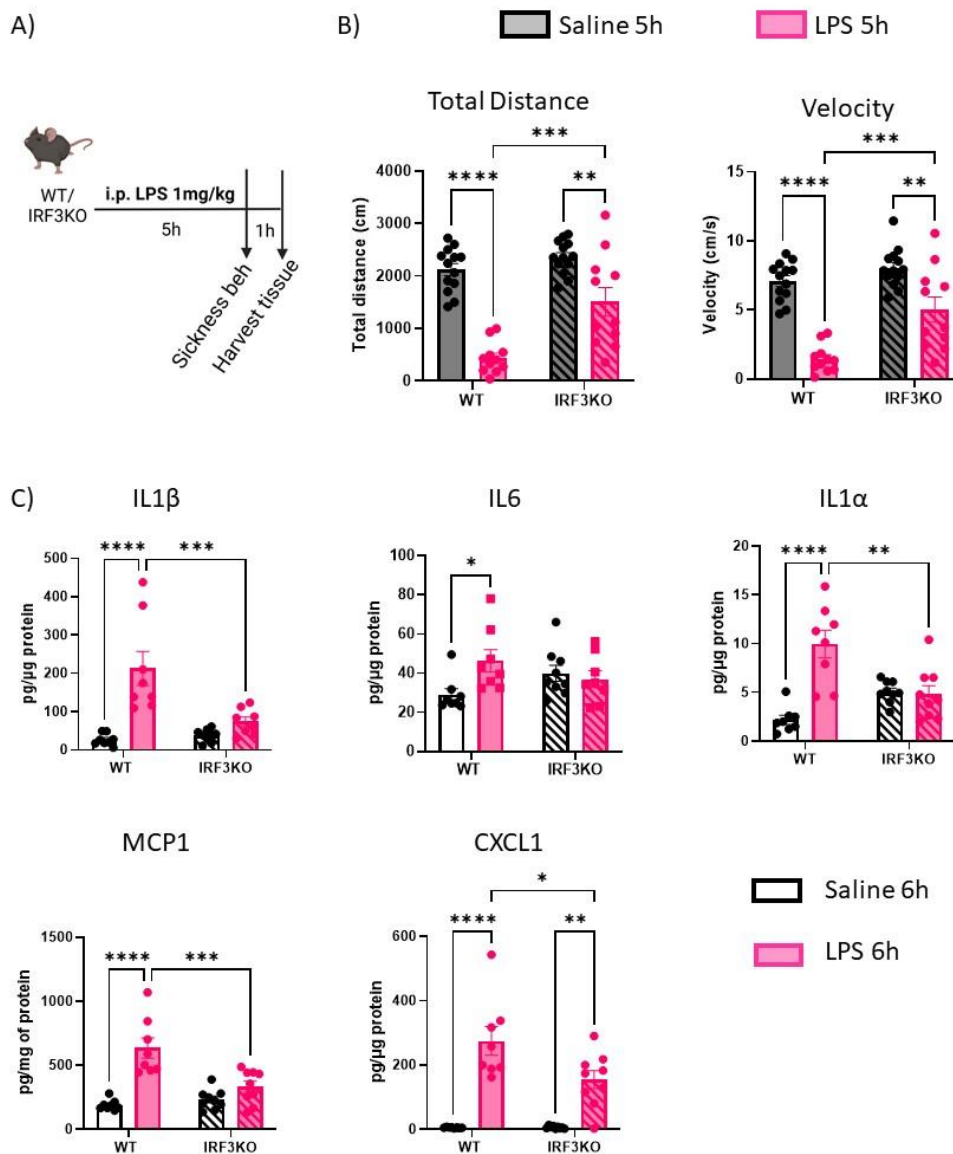
564



565 Figures:

566 **Figure 1: IRF3 deletion attenuates the proinflammatory effects of acute LPS**  
567 **challenge.**

Figure 1: IRF3 deletion attenuates the pro-inflammatory effects of acute LPS challenge.



568

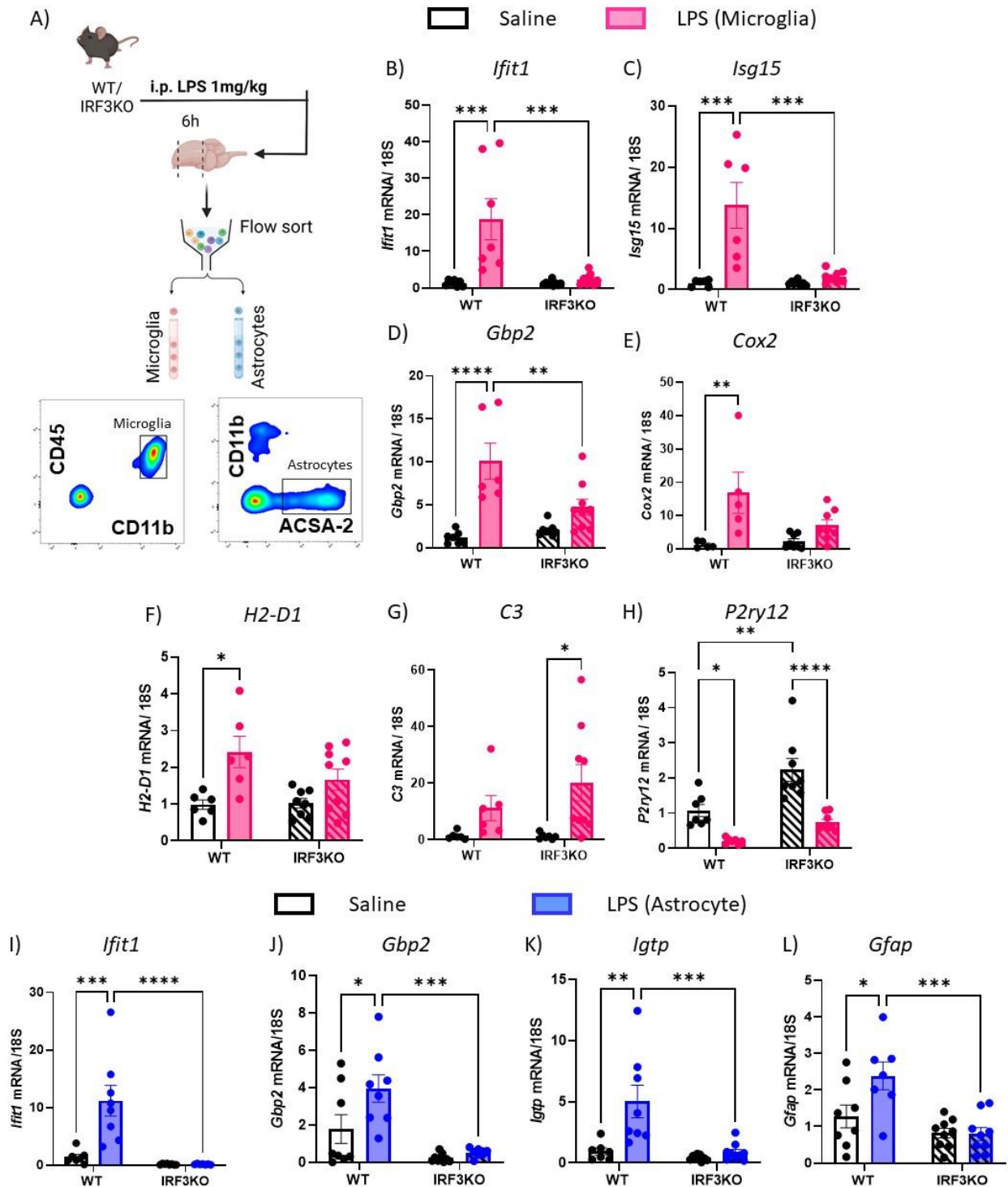
569 A) Schematic of the acute LPS challenge model. Sickness behavior was recorded in  
570 the open field arena ~5h after i.p. (intraperitoneal) LPS administration and tissue was  
571 collected after 6h.

572 B) Quantification of distance traveled and velocity of movement in open field arena  
573 shows that IRF3KO mice display attenuated sickness behavior compared to the WT.  
574 N=11-13 for each group.

575 C) Quantification of Elisa from cortical lysates shows that proinflammatory cytokines  
576 are significantly upregulated in WT mice on LPS challenge but remain significantly  
577 reduced in the IRF3KO cortices compared to the WT. N=11-13 for each group  
578 Two-way ANOVA with Tukey's multiple comparisons. \* $p < 0.05$ , \*\* $p < 0.01$ , \*\*\* $p < 0.001$ ,  
579 \*\*\*\* $p < 0.0001$

580 **Figure 2: Transcripts from microglia & astrocytes of IRF3KO mice show a**  
581 **dampened proinflammatory response to LPS.**

Figure 2 : Transcripts from microglia & astrocytes of IRF3KO mice show a dampened proinflammatory response to LPS.



582

583 A) Schematic of the protocol for isolation of microglia and astrocytes after acute LPS  
584 challenge.

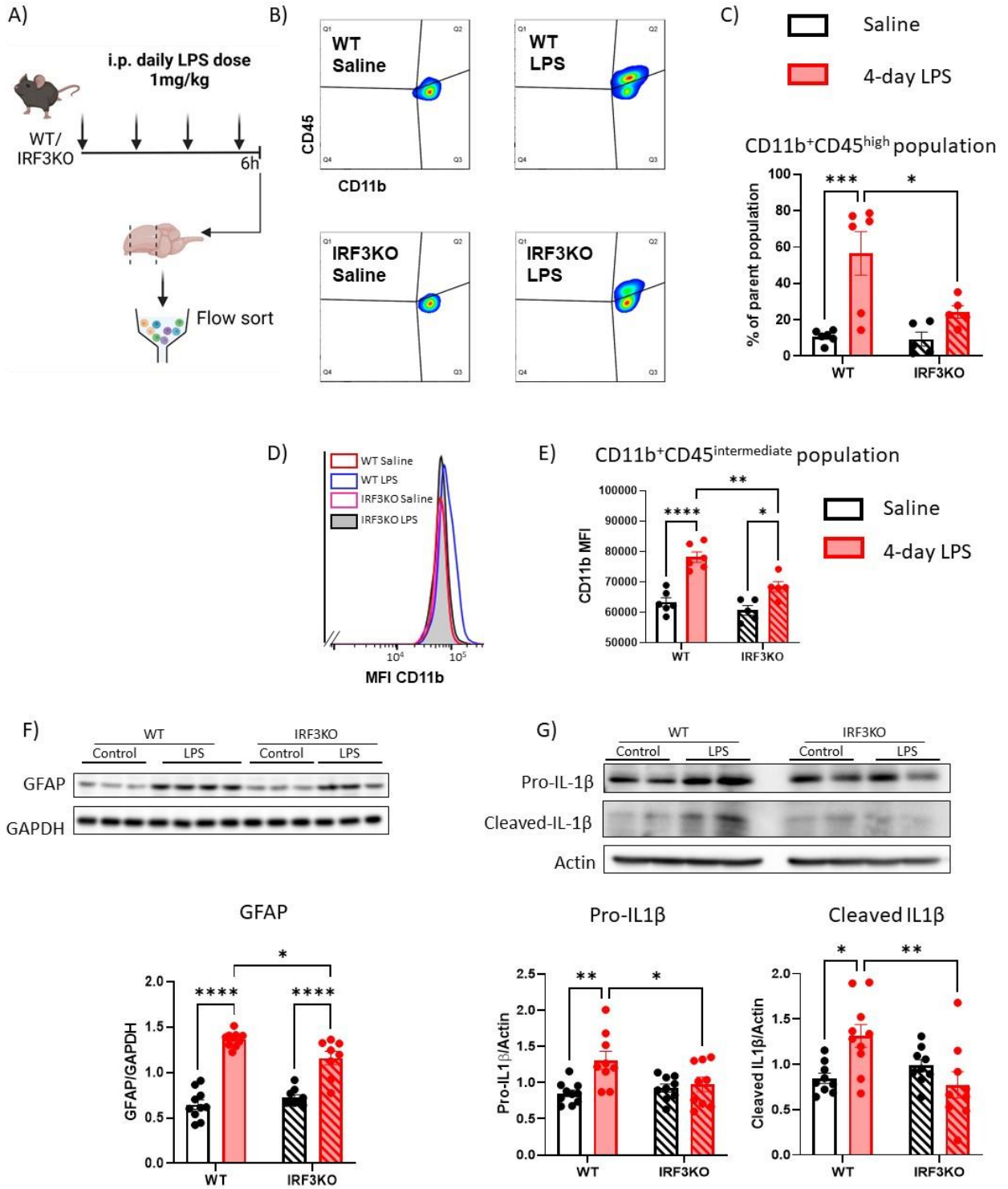
585 B-H) Quantification of qRT-PCR of transcripts from microglia show increased transcript  
586 levels of *Ifit1*, *Isg15*, *Gbp2*, *H2-D1*, and *Cox2* in WT-LPS group. While IRF3KO mice do  
587 not show significant induction of ISGs and certain proinflammatory transcripts in  
588 microglia (B-F), they appear more sensitive to LPS-mediated induction of C3 transcripts  
589 (G). Also, compared to WT, IRF3KO microglia show a similar reduction in levels of  
590 *P2ry12* (H). N=6,9 per group.

591 I-L) Quantification of qRT-PCR of transcripts (*Ifit1*, *Gbp2*, *Igtp*, *Gfap*) from astrocytes  
592 shows the attenuated response to LPS-induced transcripts compared to the WT  
593 controls. N=7,9 per group.

594 Two-way ANOVA with Tukey's multiple comparisons. \*p<0.05, \*\*p<0.01,  
595 \*\*\*p<0.001, \*\*\*\*p<0.0001

596 **Figure 3: IRF3KO mice show reduced proinflammatory changes in the brain after**  
597 **repeated LPS challenges.**

Figure 3: IRF3KO mice show reduced proinflammatory changes in the brain after repeated LPS challenges.



598

599 A) Schematic of the 4-day repeated LPS challenge paradigm.

600 B) Representative images of FACS analysis showing presence of significantly more  
601 infiltrating myeloid cells in Quadrant 2 (Q2)(CD11b<sup>+</sup>,CD45<sup>high</sup>) in the WT-LPS group in  
602 addition to the microglia population (CD11b<sup>+</sup>,CD45<sup>intermediate</sup>) in Q3.

603

604 C) Quantification of the % of infiltrating cells shows that LPS-induced infiltration of  
605 myeloid cells was markedly reduced in the IRF3KO-LPS mice compared to the WT-  
606 LPS. N=5,6 each group. The parent population is defined as live cells based on DAPI  
607 staining.

608 D-E) Quantification of the levels of mean fluorescence intensity of CD11b gated on the  
609 microglia in Q3 shows a more significant increase in WT-LPS microglia compared to  
610 IRF3KO-LPS microglia. N=5,6 each group.

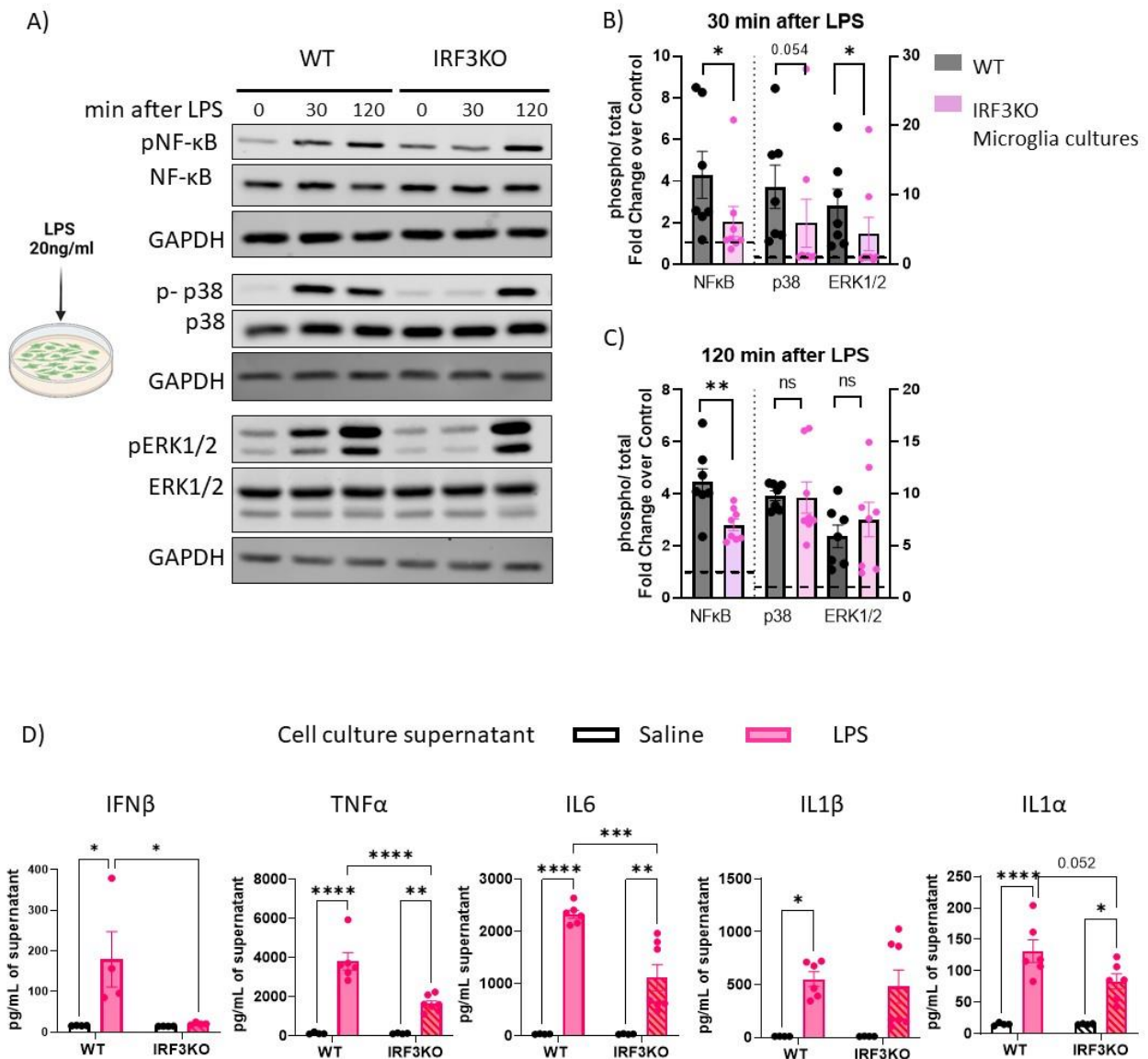
611 F) Representative images of western blots showing increased astrocyte proliferation in  
612 LPS-treated WT and IRF3KO samples in the cortical lysates. Quantification shows that  
613 the extent of astrocyte proliferation is significantly lower in IRF3KO mice compared to  
614 the WT. N=9,10 each group.

615 G) Representative images and quantification of western blots showing a significant  
616 increase in the hippocampi of pro-IL1 $\beta$  (full length) and cleaved-IL1 $\beta$  indicate activation  
617 of inflammasome in LPS-treated WT samples. Quantification shows that IRF3KO mice  
618 are protected from this increase. N=9,10 each group.

619 Two-way ANOVA with Tukey's multiple comparisons. \*p<0.05, \*\*p<0.01, \*\*\*p<0.001,  
620 \*\*\*\*p<0.0001

621 **Figure 4: IRF3 deficient primary microglia cultures show delayed downstream**  
622 **signaling and attenuated cytokine production on LPS challenge.**

Figure 4: IRF3 deficient primary microglia cultures show delayed downstream signaling and attenuated cytokine production on LPS challenge.



623

624 A) Representative images of western blots from primary microglia cultures treated  
 625 with LPS.

626

627 B) Quantification shows that 30 min after LPS stimulation, there is an increase in  
 628 phosphorylation of NF-κB, p38, and ERK1/2 as indicated by the fold change over control  
 629 of >1 in WT and IRF3KO cultures. However, IRF3KO microglia cultures show significant



630 reduction in the levels of phosphorylation compared to that of WT. N= 7,8 for each  
631 group. Mann-Whitney test, \* $p < 0.05$ , \*\* $p < 0.01$ , \*\*\* $p < 0.001$ , \*\*\*\* $p < 0.0001$ .

632

633 C) Quantification shows that 120 min after LPS stimulation, there is an increase in  
634 phosphorylation of NF- $\kappa$ B, p38, and ERK1/2 as indicated by the fold change over control  
635  $>1$  for both genotypes. However, IRF3KO microglia cultures only show a significant  
636 reduction in the levels of phosphorylation of NF- $\kappa$ B, while those of p38 and ERK1/2 are  
637 indistinguishable from that of the WT. N= 7,8 for each group. Mann-Whitney test or  
638 unpaired t-test as appropriate. \* $p < 0.05$ , \*\* $p < 0.01$ , \*\*\* $p < 0.001$ , \*\*\*\* $p < 0.0001$ .

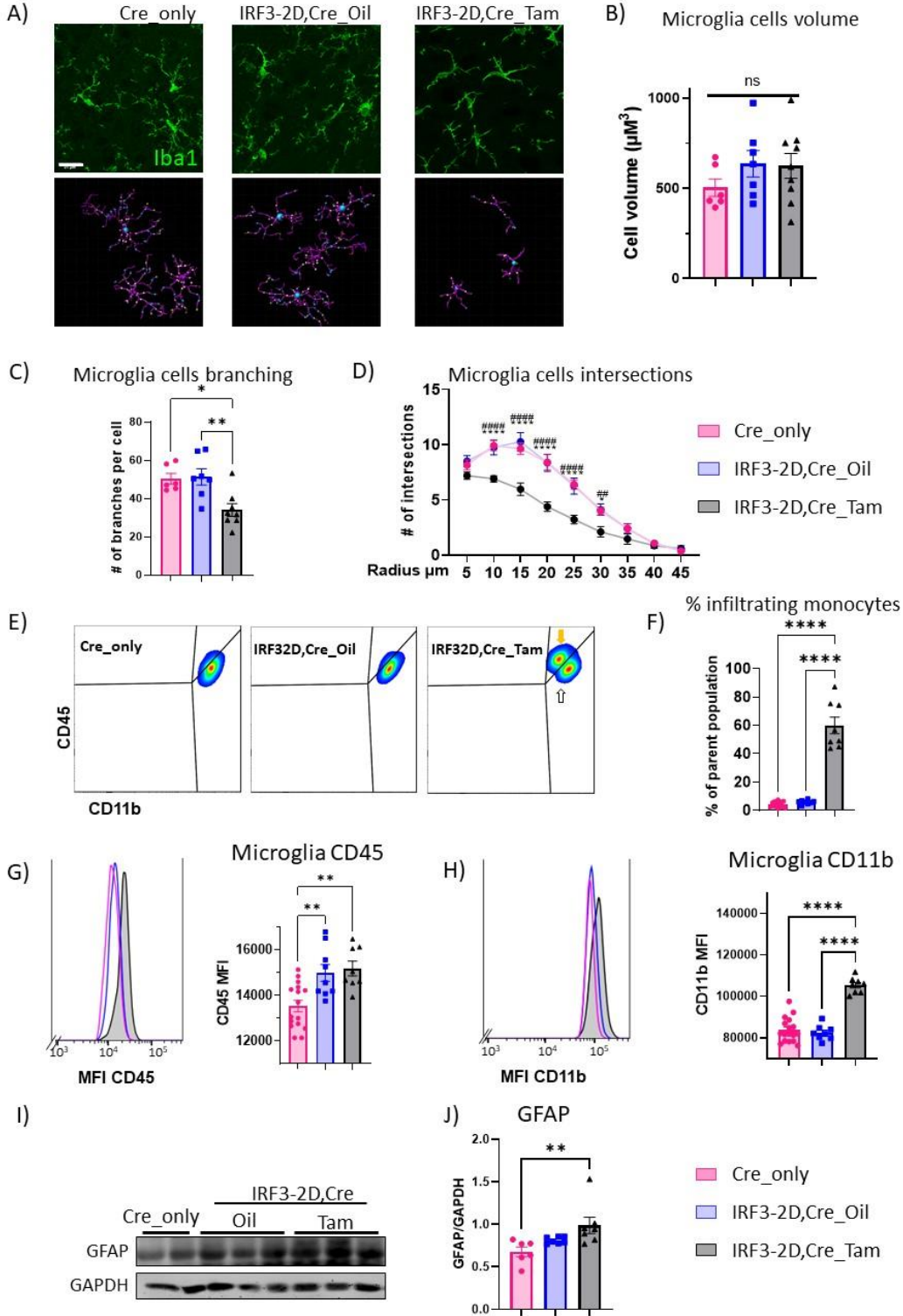
639

640 D) Quantification of Elisa from cell culture supernatants shows that proinflammatory  
641 cytokines (IFN $\beta$ , TNF $\alpha$ , IL6, IL $\beta$ , IL1 $\alpha$ ) are significantly upregulated in WT microglia on  
642 LPS challenge. IRF3KO cultures show either no release or significantly reduced release  
643 of cytokines on LPS challenge. N=4-7 for each group. Two-way ANOVA with Tukey's  
644 multiple comparisons. \* $p < 0.05$ , \*\* $p < 0.01$ , \*\*\* $p < 0.001$ , \*\*\*\* $p < 0.0001$

645

646 **Figure 5: Expression of a constitutively active form of IRF3 is sufficient to induce**  
647 **neuroinflammation.**

Figure 5 : Expression of a constitutively active form of IRF3 is sufficient to induce neuroinflammation.



649 A) Representative images of microglia (Tmem119<sup>+</sup> cells were picked) co-stained with  
650 Iba1 and Scholl analysis performed using filament tracer software from Imaris. The  
651 scale bar is 21 $\mu$ M.

652

653 B) Total volume of the cells did not change between any of the groups tested.

654

655 C) Quantification of the microglia morphology shows that microglia (Cells positive for  
656 Tmem119) from IRF3-2D,Cre\_Tam group show significantly reduced branching  
657 compared to IRF3-2D,Cre\_Oil and Cre\_only groups.

658

659 D) Microglia from IRF3-2D,Cre\_Tam group show reduced number of intersections at  
660 10-30 $\mu$ m compared to that of IRF3-2D,Cre\_Oil and Cre\_only groups. \* represents  
661 comparison with Cre\_only, # represent comparison with IRF3-2D,Cre\_Oil.

662

663 For Scholl analysis N=6-8 for each group. >7 microglia were analyzed per animal.

664 Data was analyzed using One-way ANOVA. \*p<0.05, \*\*p<0.01, \*\*\*p<0.001,  
665 \*\*\*\*p<0.000.

666

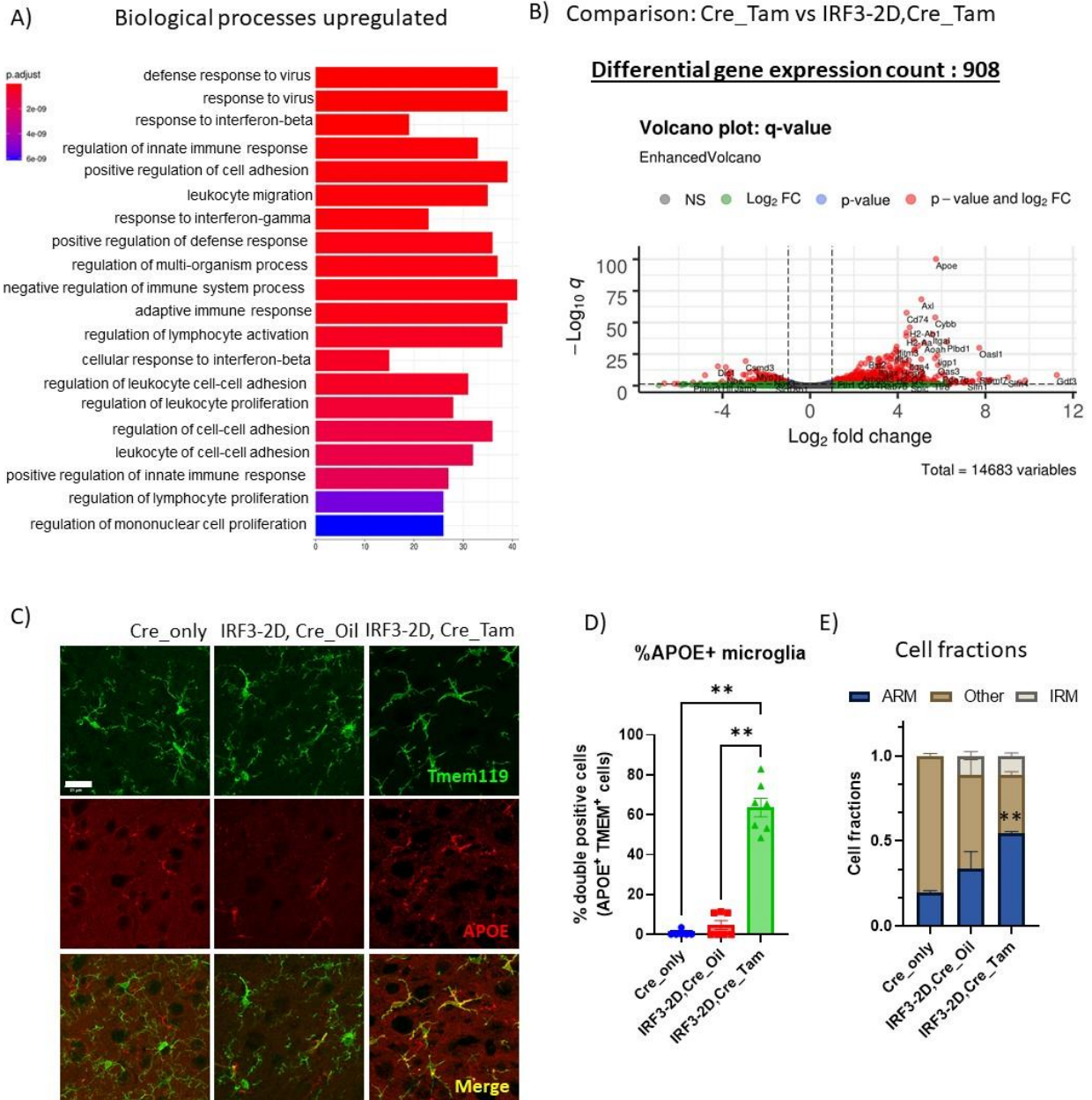
667 E-F) Representative images and quantification of FACS analysis showing the presence  
668 of infiltrating myeloid cells (CD11b<sup>+</sup>,CD45<sup>high</sup>) in the IRF3-2D,Cre\_Tam (Yellow arrow)  
669 group in addition to the microglia population (CD11b<sup>+</sup>,CD45<sup>intermediate</sup>) (White arrow). N=  
670 8,9 each group. One-way Anova with Sidak's multiple comparison test. \*\*\*\*p<0.0001

671 G-H) Quantification of CD45 and CD11b MFI gated on microglia (White arrow in E)  
672 shows significant upregulation in IRF3-2D,Cre\_Tam, suggesting more reactive state  
673 compared to Cre\_only controls. N= 8,9 each group. One-way Anova with Sidak's  
674 multiple comparison test. \*\*\*\*p<0.0001

675 I) Quantification of the western blots shows proliferation of astrocytes, as measured by  
676 GFAP levels in cortical lysates, of IRF3-2D,Cre\_Tam compared to Cre\_only. N= 6,7  
677 each group. Kruskal-Wallis test with Dunn's multiple comparison test.

678 **Figure 6: Overexpression of a constitutively active form of IRF3 leads to**  
 679 **proinflammatory phenotype and induces expression of the AD risk genes.**

Figure 6: Overexpression of a constitutively active form of IRF3 leads to proinflammatory phenotype and induces expression of the AD risk genes



680

681 A) GO analysis of the differentially upregulated genes in FACS-sorted myeloid cells  
 682 from IRF3-2D,Cre\_Tam mice compared to Cre\_only show proinflammatory phenotypes

683 and upregulation of pathways related to interferon- $\beta$ ,  $\gamma$  signaling, cell adhesion, and  
684 leukocyte proliferation.

685

686 B) Volcano plot showing differentially expressed genes in IRF3-2D,Cre\_Tam mice  
687 compared to Cre\_Tam. Note the upregulation of AD-associated genes. (n=2 for  
688 Cre\_Tam, n=3 for IRF3-2D,Cre\_Tam)

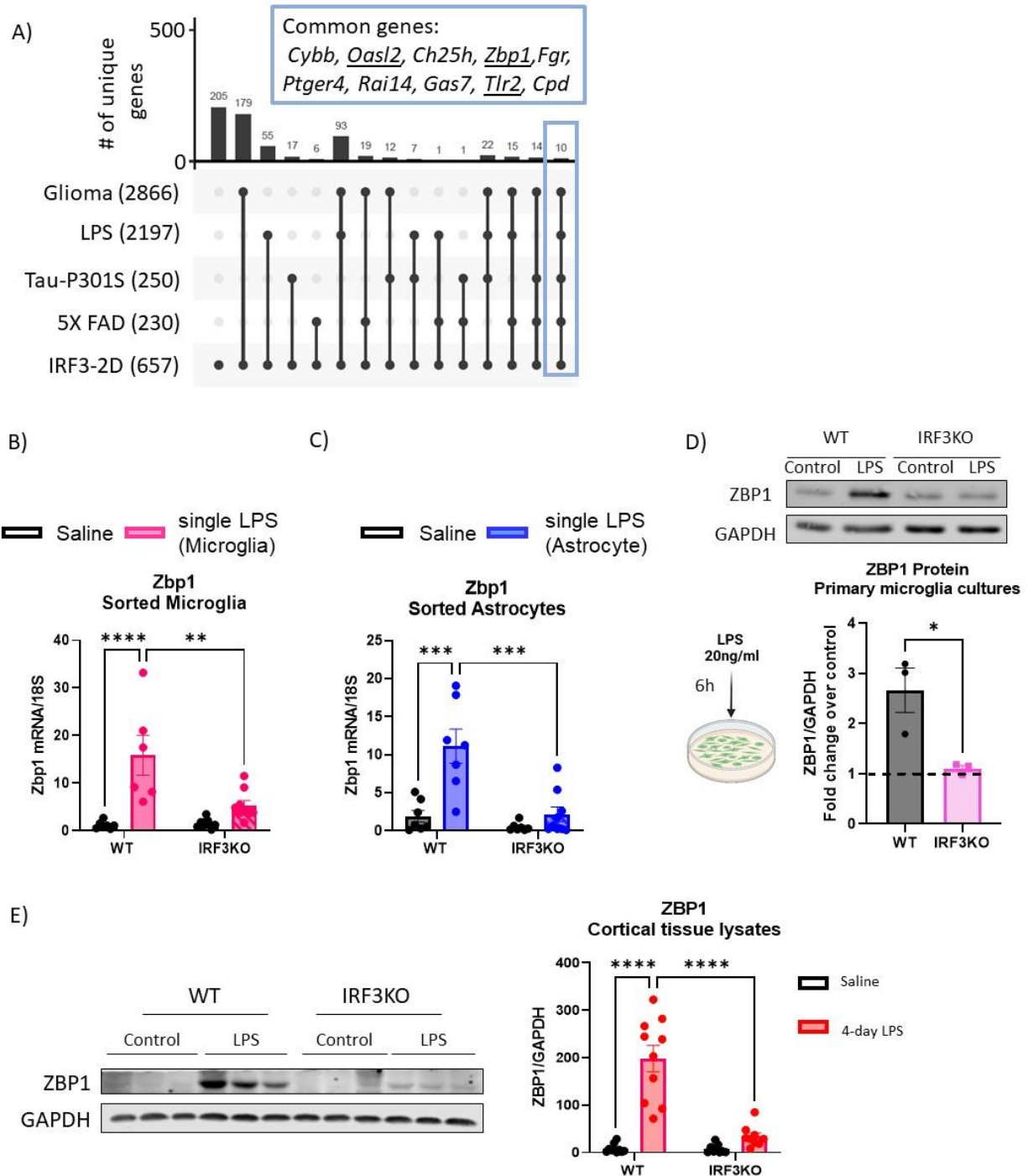
689 C-D) Representative images of APOE staining in the cortex. Quantification confirms that  
690 APOE levels are significantly upregulated in the microglia from IRF3-2D,Cre\_Tam  
691 group. The scale bar is 21 $\mu$ M. N= 6,8 per group. One-way Anova with Sidak's multiple  
692 comparison test. \*\*\*\*p<0.0001.

693 E) Deconvolution analysis on myeloid cells from IRF3-2D,Cre\_Tam mice shows  
694 significantly more ARM-like cell fraction compared to Cre\_only fraction. Both IRF3-  
695 2D,Cre\_Oil and IRF3-2D,Cre\_Tam cells contain IRM- populations in response to IRF3-  
696 2D-mediated signaling.

697

698 **Figure 7: Zbp1 is a proinflammatory transcript common across various**  
699 **neuroinflammatory conditions and its expression is regulated by IRF3.**

Figure 7: Zbp1 is a proinflammatory transcript common across various neuroinflammatory conditions and its expression is regulated by IRF3.



700

701 A) An upset plot of differentially expressed genes in IRF3-2D expressing myeloid cells  
702 and microglia from various neuroinflammatory conditions. The number of differentially



703 upregulated genes from each disease are represented in the bracket. Note the set of  
704 common genes across all five neuro-inflammatory conditions encased in blue.  
705 Underlined genes were identified as direct transcriptional targets of IRF3.

706 B-C) Quantification of qRT-PCR of microglia and astrocytes sorted from acute LPS  
707 model (6h LPS challenge in vivo) shows upregulation of Zbp1 mRNA in WT, which is  
708 absent in IRF3KO condition. N=6-9 in each group. Two-way ANOVA with Tukey's  
709 multiple comparisons. \*\*p<0.01, \*\*\*\*p<0.0001

710 D) Representative image and quantification of western blot from microglia cultures  
711 treated with LPS for 6h show 2.6 fold induction in ZBP1 in WT microglia but not IRF3KO  
712 cultures. N=3 biological replicates. Unpaired t-test. \*p<0.05

713

714 E) Western blot image and quantification of cortical tissue from WT and IRF3KO mice  
715 treated with LPS or saline for 4 days, show ZBP1 induction only in the WT-LPS group  
716 and absent in IRF3KO-LPS condition. N=9,10 each group. Two-way ANOVA with  
717 Tukey's multiple comparisons. \*\*\*\*p<0.0001

718

719

720

721



## 722 References:

- 723 1. Platanius LC. Mechanisms of type-I- and type-II-interferon-mediated signalling. *Nat Rev Immunol.*  
724 2005;5:375-86.
- 725 2. McNab F, Mayer-Barber K, Sher A, Wack A and O'Garra A. Type I interferons in infectious disease.  
726 *Nat Rev Immunol.* 2015;15:87-103.
- 727 3. Jin M, Xu R, Wang L, Alam MM, Ma Z, Zhu S, Martini AC, Jadali A, Bernabucci M, Xie P, Kwan KY,  
728 Pang ZP, Head E, Liu Y, Hart RP and Jiang P. Type-I-interferon signaling drives microglial dysfunction and  
729 senescence in human iPSC models of Down syndrome and Alzheimer's disease. *Cell Stem Cell.*  
730 2022;29:1135-1153.e8.
- 731 4. Roy ER, Wang B, Wan YW, Chiu G, Cole A, Yin Z, Propson NE, Xu Y, Jankowsky JL, Liu Z, Lee VM,  
732 Trojanowski JQ, Ginsberg SD, Butovsky O, Zheng H and Cao W. Type I interferon response drives  
733 neuroinflammation and synapse loss in Alzheimer disease. *J Clin Invest.* 2020;130:1912-1930.
- 734 5. Roy ER, Chiu G, Li S, Propson NE, Kanchi R, Wang B, Coarfa C, Zheng H and Cao W. Concerted type  
735 I interferon signaling in microglia and neural cells promotes memory impairment associated with amyloid  
736  $\beta$  plaques. *Immunity.* 2022;55:879-894.e6.
- 737 6. Barrett JP, Knobloch SM, Bhattacharya S, Gordish-Dressman H, Stoica BA and Loane DJ. Traumatic  
738 Brain Injury Induces cGAS Activation and Type I Interferon Signaling in Aged Mice. *Front Immunol.*  
739 2021;12:710608.
- 740 7. Abdullah A, Zhang M, Frugier T, Bedoui S, Taylor JM and Crack PJ. STING-mediated type-I  
741 interferons contribute to the neuroinflammatory process and detrimental effects following traumatic  
742 brain injury. *J Neuroinflammation.* 2018;15:323.
- 743 8. Kong L, Li W, Chang E, Wang W, Shen N, Xu X, Wang X, Zhang Y, Sun W, Hu W, Xu P and Liu X.  
744 mtDNA-STING Axis Mediates Microglial Polarization via IRF3/NF- $\kappa$ B Signaling After Ischemic Stroke. *Front*  
745 *Immunol.* 2022;13:860977.
- 746 9. Ben-Yehuda H, Matcovitch-Natan O, Kertser A, Spinrad A, Prinz M, Amit I and Schwartz M.  
747 Maternal Type-I interferon signaling adversely affects the microglia and the behavior of the offspring  
748 accompanied by increased sensitivity to stress. *Mol Psychiatry.* 2020;25:1050-1067.
- 749 10. Li J, Pang Y, Du Y, Xia L, Chen M, Fan Y and Dong Z. Lack of interferon regulatory factor 3 leads to  
750 anxiety/depression-like behaviors through disrupting the balance of neuronal excitation and inhibition in  
751 mice. *Genes Dis.* 2023;10:1062-1074.
- 752 11. Suzzi S, Tsitsou-Kampeli A and Schwartz M. The type I interferon antiviral response in the choroid  
753 plexus and the cognitive risk in COVID-19. *Nat Immunol.* 2023;24:220-224.
- 754 12. Crow YJ and Stetson DB. The type I interferonopathies: 10 years on. *Nat Rev Immunol.*  
755 2022;22:471-483.
- 756 13. Salih DA, Bayram S, Guelfi S, Reynolds RH, Shoai M, Ryten M, Brenton JW, Zhang D, Matarin M,  
757 Botia JA, Shah R, Brookes KJ, Guetta-Baranes T, Morgan K, Bellou E, Cummings DM, Escott-Price V and  
758 Hardy J. Genetic variability in response to amyloid beta deposition influences Alzheimer's disease risk.  
759 *Brain Commun.* 2019;1:fcz022.
- 760 14. Sala Frigerio C, Wolfs L, Fattorelli N, Thrupp N, Voytyuk I, Schmidt I, Mancuso R, Chen WT,  
761 Woodbury ME, Srivastava G, Möller T, Hudry E, Das S, Saido T, Karran E, Hyman B, Perry VH, Fiers M and  
762 De Strooper B. The Major Risk Factors for Alzheimer's Disease: Age, Sex, and Genes Modulate the  
763 Microglia Response to A $\beta$  Plaques. *Cell Rep.* 2019;27:1293-1306.e6.
- 764 15. Olah M, Menon V, Habib N, Taga MF, Ma Y, Yung CJ, Cimpean M, Khairallah A, Coronas-Samano  
765 G, Sankowski R, Grün D, Kroshilina AA, Dionne D, Sarkis RA, Cosgrove GR, Helgager J, Golden JA, Pennell  
766 PB, Prinz M, Vonsattel JPG, Teich AF, Schneider JA, Bennett DA, Regev A, Elyaman W, Bradshaw EM and  
767 De Jager PL. Single cell RNA sequencing of human microglia uncovers a subset associated with Alzheimer's  
768 disease. *Nat Commun.* 2020;11:6129.

- 769 16. Hammond TR, Dufort C, Dissing-Olesen L, Giera S, Young A, Wysoker A, Walker AJ, Gergits F, Segel  
770 M, Nemesh J, Marsh SE, Saunders A, Macosko E, Ginhoux F, Chen J, Franklin RJM, Piao X, McCarroll SA and  
771 Stevens B. Single-Cell RNA Sequencing of Microglia throughout the Mouse Lifespan and in the Injured  
772 Brain Reveals Complex Cell-State Changes. *Immunity*. 2019;50:253-271.e6.
- 773 17. Hasel P, Rose IVL, Sadick JS, Kim RD and Liddel SA. Neuroinflammatory astrocyte subtypes in  
774 the mouse brain. *Nat Neurosci*. 2021;24:1475-1487.
- 775 18. Kaya T, Mattugini N, Liu L, Ji H, Cantuti-Castelvetri L, Wu J, Schifferer M, Groh J, Martini R, Besson-  
776 Girard S, Kaji S, Liesz A, Gokce O and Simons M. CD8(+) T cells induce interferon-responsive  
777 oligodendrocytes and microglia in white matter aging. *Nat Neurosci*. 2022;25:1446-1457.
- 778 19. Honda K, Takaoka A and Taniguchi T. Type I interferon gene induction by the interferon regulatory  
779 factor family of transcription factors. *Immunity*. 2006;25:349-60.
- 780 20. Sakaguchi S, Negishi H, Asagiri M, Nakajima C, Mizutani T, Takaoka A, Honda K and Taniguchi T.  
781 Essential role of IRF-3 in lipopolysaccharide-induced interferon-beta gene expression and endotoxin  
782 shock. *Biochem Biophys Res Commun*. 2003;306:860-6.
- 783 21. Fitzgerald KA, Rowe DC, Barnes BJ, Caffrey DR, Visintin A, Latz E, Monks B, Pitha PM and Golenbock  
784 DT. LPS-TLR4 signaling to IRF-3/7 and NF-kappaB involves the toll adapters TRAM and TRIF. *J Exp Med*.  
785 2003;198:1043-55.
- 786 22. Patel SJ, Liu N, Piaker S, Gulko A, Andrade ML, Heyward FD, Sermersheim T, Edinger N, Srinivasan  
787 H, Emont MP, Westcott GP, Luther J, Chung RT, Yan S, Kumari M, Thomas R, Deleye Y, Tchernof A, White  
788 PJ, Baselli GA, Meroni M, De Jesus DF, Ahmad R, Kulkarni RN, Valenti L, Tsai L and Rosen ED. Hepatic IRF3  
789 fuels dysglycemia in obesity through direct regulation of Ppp2r1b. *Sci Transl Med*. 2022;14:eabh3831.
- 790 23. Yan S, Kumari M, Xiao H, Jacobs C, Kochumon S, Jedrychowski M, Chouchani E, Ahmad R and  
791 Rosen ED. IRF3 reduces adipose thermogenesis via ISG15-mediated reprogramming of glycolysis. *J Clin  
792 Invest*. 2021;131.
- 793 24. Zhuang Y, Ortega-Ribera M, Thevkar Nagesh P, Joshi R, Huang H, Wang Y, Zivny A, Mehta J, Parikh  
794 SM and Szabo G. Bile acid-induced IRF3 phosphorylation mediates cell death, inflammatory responses and  
795 fibrosis in cholestasis-induced liver and kidney injury via regulation of ZBP1. *Hepatology*. 2023.
- 796 25. Yanai H, Chiba S, Hangai S, Kometani K, Inoue A, Kimura Y, Abe T, Kiyonari H, Nishio J, Taguchi-  
797 Atarashi N, Mizushima Y, Negishi H, Grosschedl R and Taniguchi T. Revisiting the role of IRF3 in  
798 inflammation and immunity by conditional and specifically targeted gene ablation in mice. *Proc Natl Acad  
799 Sci U S A*. 2018;115:5253-5258.
- 800 26. Zhang Y, Chen K, Sloan SA, Bennett ML, Scholze AR, O'Keeffe S, Phatnani HP, Guarnieri P, Caneda  
801 C, Ruderisch N, Deng S, Liddel SA, Zhang C, Daneman R, Maniatis T, Barres BA and Wu JQ. An RNA-  
802 sequencing transcriptome and splicing database of glia, neurons, and vascular cells of the cerebral cortex.  
803 *J Neurosci*. 2014;34:11929-47.
- 804 27. Ma W, Oliveira-Nunes MC, Xu K, Kossenkov A, Reiner BC, Crist RC, Hayden J and Chen Q. Type I  
805 interferon response in astrocytes promotes brain metastasis by enhancing monocytic myeloid cell  
806 recruitment. *Nat Commun*. 2023;14:2632.
- 807 28. Zhu W, Cao FS, Feng J, Chen HW, Wan JR, Lu Q and Wang J. NLRP3 inflammasome activation  
808 contributes to long-term behavioral alterations in mice injected with lipopolysaccharide. *Neuroscience*.  
809 2017;343:77-84.
- 810 29. Czerkies M, Korwek Z, Prus W, Kocharczyk M, Jaruszewicz-Błońska J, Tudelska K, Błoński S, Kimmel  
811 M, Brasier AR and Lipniacki T. Cell fate in antiviral response arises in the crosstalk of IRF, NF-κB and  
812 JAK/STAT pathways. *Nat Commun*. 2018;9:493.
- 813 30. Mandrek P and Szabo G. Signaling pathways in alcohol-induced liver inflammation. *J Hepatol*.  
814 2009;50:1258-66.

- 815 31. Faust TE, Feinberg PA, O'Connor C, Kawaguchi R, Chan A, Strasburger H, Frosch M, Boyle MA,  
816 Masuda T, Amann L, Knobloch KP, Prinz M, Schaefer A and Schafer DP. A comparative analysis of  
817 microglial inducible Cre lines. *Cell Rep.* 2023;42:113031.
- 818 32. Krasemann S, Madore C, Cialic R, Baufeld C, Calcagno N, El Fatimy R, Beckers L, O'Loughlin E, Xu  
819 Y, Fanek Z, Greco DJ, Smith ST, Tweet G, Humulock Z, Zrzavy T, Conde-Sanroman P, Gacias M, Weng Z,  
820 Chen H, Tjon E, Mazaheri F, Hartmann K, Madi A, Ulrich JD, Glatzel M, Worthmann A, Heeren J, Budnik B,  
821 Lemere C, Ikezu T, Heppner FL, Litvak V, Holtzman DM, Lassmann H, Weiner HL, Ochoa J, Haass C and  
822 Butovsky O. The TREM2-APOE Pathway Drives the Transcriptional Phenotype of Dysfunctional Microglia  
823 in Neurodegenerative Diseases. *Immunity.* 2017;47:566-581 e9.
- 824 33. Deczkowska A, Keren-Shaul H, Weiner A, Colonna M, Schwartz M and Amit I. Disease-Associated  
825 Microglia: A Universal Immune Sensor of Neurodegeneration. *Cell.* 2018;173:1073-1081.
- 826 34. Keren-Shaul H, Spinrad A, Weiner A, Matcovitch-Natan O, Dvir-Szternfeld R, Ulland TK, David E,  
827 Baruch K, Lara-Astaiso D, Toth B, Itzkovitz S, Colonna M, Schwartz M and Amit I. A Unique Microglia Type  
828 Associated with Restricting Development of Alzheimer's Disease. *Cell.* 2017;169:1276-1290 e17.
- 829 35. Friedman BA, Srinivasan K, Ayalon G, Meilandt WJ, Lin H, Huntley MA, Cao Y, Lee SH, Haddick PCG,  
830 Ngu H, Modrusan Z, Larson JL, Kaminker JS, van der Brug MP and Hansen DV. Diverse Brain Myeloid  
831 Expression Profiles Reveal Distinct Microglial Activation States and Aspects of Alzheimer's Disease Not  
832 Evident in Mouse Models. *Cell Rep.* 2018;22:832-847.
- 833 36. Kuriakose T and Kanneganti TD. ZBP1: Innate Sensor Regulating Cell Death and Inflammation.  
834 *Trends Immunol.* 2018;39:123-134.
- 835 37. Muendlein HI, Connolly WM, Magri Z, Jetton D, Smirnova I, Degtarev A, Balachandran S and  
836 Poltorak A. ZBP1 promotes inflammatory responses downstream of TLR3/TLR4 via timely delivery of RIPK1  
837 to TRIF. *Proc Natl Acad Sci U S A.* 2022;119:e2113872119.
- 838 38. Petrasek J, Iracheta-Vellve A, Csak T, Satishchandran A, Kodys K, Kurt-Jones EA, Fitzgerald KA and  
839 Szabo G. STING-IRF3 pathway links endoplasmic reticulum stress with hepatocyte apoptosis in early  
840 alcoholic liver disease. *Proc Natl Acad Sci U S A.* 2013;110:16544-9.
- 841 39. Andersen LL, Mørk N, Reinert LS, Kofod-Olsen E, Narita R, Jørgensen SE, Skipper KA, Höning K, Gad  
842 HH, Østergaard L, Ørntoft TF, Hornung V, Paludan SR, Mikkelsen JG, Fujita T, Christiansen M, Hartmann R  
843 and Mogensen TH. Functional IRF3 deficiency in a patient with herpes simplex encephalitis. *J Exp Med.*  
844 2015;212:1371-9.
- 845 40. Canivet C, Rhéaume C, Lebel M, Piret J, Gosselin J and Boivin G. Both IRF3 and especially IRF7 play  
846 a key role to orchestrate an effective cerebral inflammatory response in a mouse model of herpes simplex  
847 virus encephalitis. *J Neurovirol.* 2018;24:761-768.
- 848 41. Schultz KLW, Troisi EM, Baxter VK, Glowinski R and Griffin DE. Interferon regulatory factors 3 and  
849 7 have distinct roles in the pathogenesis of alphavirus encephalomyelitis. *J Gen Virol.* 2019;100:46-62.
- 850 42. Salvador AF, de Lima KA and Kipnis J. Neuromodulation by the immune system: a focus on  
851 cytokines. *Nat Rev Immunol.* 2021;21:526-541.
- 852 43. Dantzer R. Cytokine, sickness behavior, and depression. *Neurol Clin.* 2006;24:441-60.
- 853 44. Calvo-Rodríguez M, García-Rodríguez C, Villalobos C and Núñez L. Role of Toll Like Receptor 4 in  
854 Alzheimer's Disease. *Front Immunol.* 2020;11:1588.
- 855 45. Heidari A, Yazdanpanah N and Rezaei N. The role of Toll-like receptors and neuroinflammation in  
856 Parkinson's disease. *J Neuroinflammation.* 2022;19:135.
- 857 46. Zheng C, Chen J, Chu F, Zhu J and Jin T. Inflammatory Role of TLR-MyD88 Signaling in Multiple  
858 Sclerosis. *Front Mol Neurosci.* 2019;12:314.
- 859 47. Lee JY, Lee JD, Phipps S, Noakes PG and Woodruff TM. Absence of toll-like receptor 4 (TLR4)  
860 extends survival in the hSOD1 G93A mouse model of amyotrophic lateral sclerosis. *J Neuroinflammation.*  
861 2015;12:90.
- 862 48. Kawasaki T and Kawai T. Toll-like receptor signaling pathways. *Front Immunol.* 2014;5:461.

- 863 49. Kim S, Kim SY, Pribis JP, Lotze M, Mollen KP, Shapiro R, Loughran P, Scott MJ and Billiar TR.  
864 Signaling of high mobility group box 1 (HMGB1) through toll-like receptor 4 in macrophages requires CD14.  
865 *Mol Med*. 2013;19:88-98.
- 866 50. Peek V, Harden LM, Damm J, Aslani F, Leisengang S, Roth J, Gerstberger R, Meurer M, von Köckritz-  
867 Blickwede M, Schulz S, Spengler B and Rummel C. LPS Primes Brain Responsiveness to High Mobility Group  
868 Box-1 Protein. *Pharmaceuticals (Basel)*. 2021;14.
- 869 51. Hritz I, Mandrekar P, Velayudham A, Catalano D, Dolganiuc A, Kodys K, Kurt-Jones E and Szabo G.  
870 The critical role of toll-like receptor (TLR) 4 in alcoholic liver disease is independent of the common TLR  
871 adapter MyD88. *Hepatology*. 2008;48:1224-31.
- 872 52. Hopfner KP and Hornung V. Molecular mechanisms and cellular functions of cGAS-STING  
873 signalling. *Nat Rev Mol Cell Biol*. 2020;21:501-521.
- 874 53. Motwani M, Pesiridis S and Fitzgerald KA. DNA sensing by the cGAS-STING pathway in health and  
875 disease. *Nat Rev Genet*. 2019;20:657-674.
- 876 54. Hou Y, Wei Y, Lautrup S, Yang B, Wang Y, Cordonnier S, Mattson MP, Croteau DL and Bohr VA.  
877 NAD(+) supplementation reduces neuroinflammation and cell senescence in a transgenic mouse model of  
878 Alzheimer's disease via cGAS-STING. *Proc Natl Acad Sci U S A*. 2021;118.
- 879 55. Käufer C, Chhatbar C, Bröer S, Waltl I, Ghita L, Gerhäuser I, Kalinke U and Löscher W. Chemokine  
880 receptors CCR2 and CX3CR1 regulate viral encephalitis-induced hippocampal damage but not seizures.  
881 *Proc Natl Acad Sci U S A*. 2018;115:E8929-e8938.
- 882 56. Heneka MT, Kummer MP, Stutz A, Delekate A, Schwartz S, Vieira-Saecker A, Griep A, Axt D, Remus  
883 A, Tzeng TC, Gelpi E, Halle A, Korte M, Latz E and Golenbock DT. NLRP3 is activated in Alzheimer's disease  
884 and contributes to pathology in APP/PS1 mice. *Nature*. 2013;493:674-8.
- 885 57. Zhou K, Shi L, Wang Y, Chen S and Zhang J. Recent Advances of the NLRP3 Inflammasome in Central  
886 Nervous System Disorders. *J Immunol Res*. 2016;2016:9238290.
- 887 58. Li N, Zhou H, Wu H, Wu Q, Duan M, Deng W and Tang Q. STING-IRF3 contributes to  
888 lipopolysaccharide-induced cardiac dysfunction, inflammation, apoptosis and pyroptosis by activating  
889 NLRP3. *Redox Biol*. 2019;24:101215.
- 890 59. Baxter PS, Dando O, Emelianova K, He X, McKay S, Hardingham GE and Qiu J. Microglial identity  
891 and inflammatory responses are controlled by the combined effects of neurons and astrocytes. *Cell Rep*.  
892 2021;34:108882.
- 893 60. Li W, Viengkhou B, Denyer G, West PK, Campbell IL and Hofer MJ. Microglia have a more extensive  
894 and divergent response to interferon- $\alpha$  compared with astrocytes. *Glia*. 2018;66:2058-2078.
- 895 61. Morrison DC and Kline LF. Activation of the classical and properdin pathways of complement by  
896 bacterial lipopolysaccharides (LPS). *J Immunol*. 1977;118:362-8.
- 897 62. Lee S, Devanney NA, Golden LR, Smith CT, Schwartz JL, Walsh AE, Clarke HA, Goulding DS, Allenger  
898 EJ, Morillo-Segovia G, Friday CM, Gorman AA, Hawkinson TR, MacLean SM, Williams HC, Sun RC, Morganti  
899 JM and Johnson LA. APOE modulates microglial immunometabolism in response to age, amyloid  
900 pathology, and inflammatory challenge. *Cell Rep*. 2023;42:112196.
- 901 63. Ulrich JD, Ulland TK, Mahan TE, Nyström S, Nilsson KP, Song WM, Zhou Y, Reinartz M, Choi S, Jiang  
902 H, Stewart FR, Anderson E, Wang Y, Colonna M and Holtzman DM. ApoE facilitates the microglial response  
903 to amyloid plaque pathology. *J Exp Med*. 2018;215:1047-1058.
- 904 64. Shi Y, Manis M, Long J, Wang K, Sullivan PM, Remolina Serrano J, Hoyle R and Holtzman DM.  
905 Microglia drive APOE-dependent neurodegeneration in a tauopathy mouse model. *J Exp Med*.  
906 2019;216:2546-2561.
- 907 65. Sahasrabudhe V and Ghosh HS. Cx3Cr1-Cre induction leads to microglial activation and IFN-1  
908 signaling caused by DNA damage in early postnatal brain. *Cell Rep*. 2022;38:110252.
- 909 66. Peng R, Wang CK, Wang-Kan X, Idorn M, Kjaer M, Zhou FY, Fiil BK, Timmermann F, Orozco SL,  
910 McCarthy J, Leung CS, Lu X, Bagola K, Rehwinkel J, Oberst A, Maelfait J, Paludan SR and Gyrd-Hansen M.

911 Human ZBP1 induces cell death-independent inflammatory signaling via RIPK3 and RIPK1. *EMBO Rep.*  
912 2022;23:e55839.  
913 67. Guo H, Chen R, Li P, Yang Q and He Y. ZBP1 mediates the progression of Alzheimer's disease via  
914 pyroptosis by regulating IRF3. *Mol Cell Biochem.* 2023.  
915 68. Marsh SE, Walker AJ, Kamath T, Dissing-Olesen L, Hammond TR, de Soysa TY, Young AMH, Murphy  
916 S, Abdulraouf A, Nadaf N, Dufort C, Walker AC, Lucca LE, Kozareva V, Vanderburg C, Hong S, Bulstrode H,  
917 Hutchinson PJ, Gaffney DJ, Hafler DA, Franklin RJM, Macosko EZ and Stevens B. Dissection of artifactual  
918 and confounding glial signatures by single-cell sequencing of mouse and human brain. *Nat Neurosci.*  
919 2022;25:306-316.  
920 69. Friker LL, Scheiblich H, Hochheiser IV, Brinkschulte R, Riedel D, Latz E, Geyer M and Heneka MT.  
921  $\beta$ -Amyloid Clustering around ASC Fibrils Boosts Its Toxicity in Microglia. *Cell Rep.* 2020;30:3743-3754.e6.  
922  
923

924

925 Funding: This study was supported by NIH grant-R01AG072899 and NIAAA grant-  
926 5R01AA017729.

927 Acknowledgments: We would like to thank NIH and NIAAA grants for funding and support.  
928 Figures-schematics were created using BioRender.com. We would like to thank Dr. Evan  
929 Rosen for generous gift of IRF3-2D (C57BL/6-Gt(ROSA)26Sortm4(CAG-  
930 Irf3\*S388D\*S390D)Evdr/J-036261) mice.

931 Disclosures:

932 GS was the editor-in-Chief of Hepatology Communication., consults for Cyta  
933 Therapeutics, Durect, Evive, Merck, Novartis, Pandion Therapeutics, Pfizer, Surrozen  
934 and Terra Firma, received royalties from UptoDate and Springer and also holds equity in  
935 Glympse Bio, Zomagen and Satellite Bio.